ALLERGY

Human airway mast cells proliferate and acquire distinct inflammation-driven phenotypes during type 2 inflammation

Daniel F. Dwyer[1,2]*, Jose Ordovas-Montanes[3,4,5,6]*, Samuel J. Allon[5,7,8], Kathleen M. Buchheit[1,2], Marko Vukovic[5,7,8], Tahereh Derakhshan[1,2], Chunli Feng[1,2], Juying Lai[1,2], Travis K. Hughes[5,7,8], Sarah K. Nyquist[5,7,8,9], Matthew P. Giannetti[1,2], Bonnie Berger[10], Neil Bhattacharyya[2,11], Rachel E. Roditi[2,11], Howard R. Katz[1,2], Martijn C. Nawijn[12,13], Marijn Berg[12,13], Maarten van den Berge[12,14], Tanya M. Laidlaw[1,2], Alex K. Shalek[5,7,8†‡], Nora A. Barrett[1,2,4†‡], Joshua A. Boyce[1,2,4†‡§]

Mast cells (MCs) play a pathobiologic role in type 2 (T2) allergic inflammatory diseases of the airway, including asthma and chronic rhinosinusitis with nasal polyposis (CRSwNP). Distinct MC subsets infiltrate the airway mucosa in T2 disease, including subepithelial MCs expressing the proteases tryptase and chymase (MC_{TC}) and epithelial MCs expressing tryptase without chymase (MC_T). However, mechanisms underlying MC expansion and the transcriptional programs underlying their heterogeneity are poorly understood. Here, we use flow cytometry and single-cell RNA-sequencing (scRNA-seq) to conduct a comprehensive analysis of human MC hyperplasia in CRSwNP, a T2 cytokine–mediated inflammatory disease. We link discrete cell surface phenotypes to the distinct transcriptomes of CRSwNP MC_T and MC_{TC}, which represent polarized ends of a transcriptional gradient of nasal polyp MCs. We find a subepithelial population of $CD38^{high}CD117^{high}$ MCs that is markedly expanded during T2 inflammation. These $CD38^{high}CD117^{high}$ MCs exhibit an intermediate phenotype relative to the expanded MC_T and MC_{TC} subsets. $CD38^{high}CD117^{high}$ MCs are distinct from circulating MC progenitors and are enriched for proliferation, which is markedly increased in CRSwNP patients with aspirin-exacerbated respiratory disease, a severe disease subset characterized by increased MC burden and elevated MC activation. We observe that MCs expressing a polyp MC_T–like effector program are also found within the lung during fibrotic diseases and asthma, and further identify marked differences between MC_{TC} in nasal polyps and skin. These results indicate that MCs display distinct inflammation-associated effector programs and suggest that in situ MC proliferation is a major component of MC hyperplasia in human T2 inflammation.

INTRODUCTION

Mast cells (MCs) are found in all barrier tissue sites under homeostatic conditions, where they are critical for host defense against helminths, viruses, bacteria, and xenobiotic venoms (*1*). MC expansion occurs across a spectrum of diseases associated with type 2 (T2) inflammation, including asthma, food allergy, eosinophilic esophagitis (EoE), and atopic dermatitis. MCs participate in T2 inflammatory disease progression and severity through eicosanoid biosynthesis, cytokine production, and the release of preformed mediators, including histamine and proteases (*1*–*3*). Pharmacologic inhibition of the MC survival receptor CD117 using imatinib reduces airway hyperresponsiveness in subjects with refractory asthma but only modestly decreases lung MC burden (*2*). Thus, developing a better mechanistic understanding of MC hyperplasia in human diseases may enable more directed and effective approaches for targeting MC-dependent pathobiology.

Two major human MC subtypes distinguished by tissue microlocalization and histologically defined protease expression patterns have been recognized within barrier tissues. Subepithelial MCs coexpress the proteases tryptase and chymase (MC_{TC}) in conjunction with cathepsin G and carboxypeptidase A3 (CPA3). Mucosal epithelial MCs express tryptase but lack chymase, cathepsin G, and CPA3 (MC_T) (*4*, *5*). Rodent studies demonstrate that subepithelial compartments are seeded by fetal-derived β7 integrin (Itgβ7)–expressing MC progenitors (MC_P) that maintain the MC populations in these locations through adulthood (*6*, *7*). In contrast, mucosal epithelial MCs arise from adult bone marrow–derived Itgβ7-expressing MC_P (*8*–*10*). Both the fetal and adult bone marrow–derived murine MC compartments are strongly influenced by local microenvironments, with fetal-derived MCs expressing tissue-specific transcriptional programs (*11*) and both MC classes exhibiting tissue-dependent protease expression profiles (*12*). Although a committed

[1]Jeff and Penny Vinik Immunology Center, Division of Allergy and Clinical Immunology, Brigham and Women's Hospital, Boston, MA, USA. [2]Department of Medicine, Harvard Medical School, Boston, MA, USA. [3]Division of Gastroenterology, Boston Children's Hospital, Boston, MA, USA. [4]Program in Immunology, Harvard Medical School, Boston, MA, USA. [5]Broad Institute of MIT and Harvard, Cambridge, MA, USA. [6]Harvard Stem Cell Institute, Cambridge, MA, USA. [7]Institute for Medical Engineering and Science (IMES), Department of Chemistry, and Koch Institute for Integrative Cancer Research, MIT, Cambridge, MA, USA. [8]Ragon Institute of MGH, MIT and Harvard, Cambridge, MA, USA. [9]Program in Computational and Systems Biology, MIT, Cambridge, MA, USA. [10]Computer Science and Artificial Intelligence Lab and Department of Mathematics, MIT, Cambridge, MA, USA. [11]Department of Surgery, Brigham and Women's Hospital, Boston, MA, USA. [12]Groningen Research Institute for Asthma and COPD, University Medical Center Groningen, University of Groningen, Groningen, Netherlands. [13]Department of Pathology and Medical Biology, Laboratory of Experimental Immunology and Respiratory Research (EXPIRE), University Medical Center Groningen, University of Groningen, Groningen, Netherlands. [14]Department of Pulmonary Diseases, University Medical Center Groningen, University of Groningen, Groningen, Netherlands.
*These authors contributed equally to this work.
†Corresponding author. Email: shalek@mit.edu (A.K.S.); jboyce@rics.bwh.harvard.edu (J.A.B.); nbarrett@bwh.harvard.edu (N.A.B.)
‡These authors contributed equally to this work.
§Lead contact.

human MC_P expressing CD34 and Itgβ7 exists in adult peripheral blood (*13*) and fetal cord blood (*14*), how mature human tissue MCs are maintained and the degree to which human MCs exhibit tissue-specific phenotypes are unknown.

T2 inflammatory airway disease markedly changes the number, distribution, phenotype, and likely the functional characteristics of MCs. Mild to moderate asthma, EoE, and chronic rhinosinusitis (CRS) with nasal polyps (CRSwNP) all involve expansion of an intraepithelial MC_T population expressing CPA3, suggesting a common paradigm underlying human mucosal T2 inflammation and a broader "inflammatory MC_T" effector program (*15*–*18*). In asthma, the concentrations of these inflammatory MC_T correlate with epithelial T2-induced gene signatures and therapeutic responses to inhaled glucocorticoids, whereas in EoE, these inflammatory MC_T exhibit degranulation during active disease (*15*, *18*). The airway smooth muscle of severe asthmatics is additionally infiltrated by MC_{TC}, where their concentration correlates with disease severity and airway hyperresponsiveness (*16*, *19*, *20*). MC_{TC} also expand in subepithelial glandular tissue in CRSwNP (*17*). Although the differential effector programs of these MC phenotypes are largely unknown, MCs harvested from polyp epithelium have decreased sensitivity to immunoglobulin E (IgE)–mediated activation relative to those from the subepithelium (*21*), indicating broader functional differences accompanying protease phenotypes. Although the expanded nasal polyp MC pool likely shares key features with that observed across human mucosal T2 inflammation, the determinants of this MC expansion and phenotypic alterations remain largely unknown.

We recently used single-cell RNA-sequencing (scRNA-seq) to deconstruct inflammatory circuits across epithelial, stromal, and immune cells in nasal polyposis, identifying MCs as a source of both T2 inflammatory cytokines (*IL5* and *IL13*) and lipid mediator biosynthetic enzymes (*ALOX5*, *ALOX5AP*, and *HPGDS*) (*22*). Here, we use directed scRNA-seq, CITE-seq (cellular indexing of transcriptomes and epitopes by sequencing), and flow cytometry to comprehensively characterize human MC phenotypes and hyperplasia within sinonasal tissues from patients with CRS with differing degrees of disease severity. Through this approach, we identify distinct cell surface phenotypes and respiratory inflammation–linked transcript expression patterns associated with a nasal polyp intraepithelial MC_T program also found in inflamed lung and subepithelial MC_{TC}s highly distinct from those found in the skin..

Our scRNA-seq results further suggest that these divergent polyp MC_T ($CD38^{high}CD117^{low}$) and MC_{TC} ($CD38^{low}CD117^{high}$) phenotypes represent two polarized states along a gradient of MC transcript and protein expression, linked by a $CD38^{high}CD117^{high}$ intermediate MC. These $CD38^{high}CD117^{high}$ MCs, present at low concentration in control tissue from patients with CRS without nasal polyps (CRSsNP), are substantially expanded in CRSwNP tissue. This expansion is associated with local proliferation, a process that is significantly increased in tissue from patients with aspirin-exacerbated respiratory disease (AERD), a severe CRSwNP disease variant associated with asthma, rapid nasal polyp growth, and high concentrations of MC activation products in biological fluids (*23*). Thus, our findings identify T2 inflammation–associated MC_T and MC_{TC} phenotypes, characterize an intermediate tissue-resident $CD38^{high}$ $CD117^{high}$ MC transcriptionally linked to both archetypal MC subsets present in polyposis, and suggest that MC hyperplasia found in this T2 disease arises, in part, from local MC proliferation.

RESULTS

Characterization of the expanded MC population in T2 inflammation

Consistent with prior studies (*24*), flow cytometric analysis demonstrated a prominent population of $CD45^+$lin(CD3, CD19, and CD11b CD11c)$^-$Fcε$R1\alpha^+CD117^+$ MCs in human nasal polyps that was expanded relative to control tissue from patients with CRSsNP (Fig. 1A). Because patients with nasal polyposis included both aspirin-tolerant individuals and patients with AERD, we further assessed MC concentration between these clinical phenotypes. We noted a significant increase in MC concentration as both percentage of $CD45^+$ and percentage of all live cells in AERD versus CRSwNP and in both polyp populations relative to CRSsNP (Fig. 1B). Thus, MC expansion occurred proportionately to disease severity.

Nasal polyp MCs exhibited more heterogeneous CD117 expression and side-angle light scatter (SSC) than CRSsNP MCs (Fig. 1C), suggesting the presence of one or more additional MC subsets in CRSwNP. Upon fractionating superficial epithelium to analyze intraepithelial MCs, we noted that these MCs were $CD117^{low}SSC^{low}$, in contrast to unfractionated polyp (Fig. 1D). On the basis of this observation, we created a flow cytometric gating scheme to distinguish $CD117^{low}SSC^{low}$ MCs from $CD117^{high}$ MCs (Fig. 1E) and confirmed a highly significant epithelial enrichment for $CD117^{low}SSC^{low}$ MCs, indicating that $CD117^{high}$ MCs were predominantly subepithelial (Fig. 1F). Epithelial MCs expressed significantly lower Fcε$R1\alpha$ than subepithelial MCs (Fig. 1G) and lacked both C-C chemokine receptor 3 (CCR3) and human leukocyte antigen class II histocompatibility antigen, DR alpha chain (HLA-DRA) despite detection of both proteins in $CD45^+$ $CD117^-$ cells, indicating no basophils or dendritic cell (DC) contamination (fig. S1, C to F). In addition, no clear population expressing the stem cell lineage marker CD34 was detected within the polyp MC pool (fig. S1G).

We next sorted $CD117^{low}$ SSC^{low} epithelial and $CD117^{high}$ subepithelial MCs for microscopic characterization. MCs within the epithelial-enriched gate contained metachromatic granules (Fig. 1H, left) and expressed tryptase with a granular staining pattern (Fig. 1H, right, channel series shown in fig. S2A), indicating a mature MC_T phenotype. MCs within the subepithelial gate contained a mix of large cells with dense metachromatic granules and smaller less granulated cells with an immature morphology (Fig. 1I, left), suggesting that the range of SSC observed within this gate reflected granular heterogeneity (Fig. 1G). Protease immunostaining indicated that the subepithelial MC pool contained cells coexpressing tryptase and chymase, indicating an MC_{TC} phenotype, as well as MCs exhibiting diffuse tryptase staining without chymase (Fig. 1I, right, channel series shown in fig. S2B). Consistent with previous studies (*17*), immunohistologic assessment confirmed that chymase-expressing cells were largely restricted to polyp subepithelium (fig. S2, C and D). Thus, MCs within the epithelial gate were MC_T characterized by reduced expression of the high-affinity IgE receptor FcεRIα and CD117, whereas subepithelial polyp MCs, exhibiting increased Fcε$R1\alpha$ and CD117, were a mix of MC_{TC} and morphologically immature MCs.

Given the presence of immature-appearing MCs, we next assessed whether $Itg\beta7^+CD34^+$ human MC_Ps might participate in polyp MC hyperplasia (*13*). A subset of SSC^{low} MCs expressing Itgβ7 ($Itg\beta7^{high}$) was observed within both the epithelial and subepithelial gates (Fig. 2A). Polyp $Itg\beta7^{high}$ MCs exhibited diffuse tryptase staining and, in contrast to the previously described circulating MC_P, contained distinct metachromatic granules (Fig. 2B). $Itg\beta7^{high}$ MCs were virtually

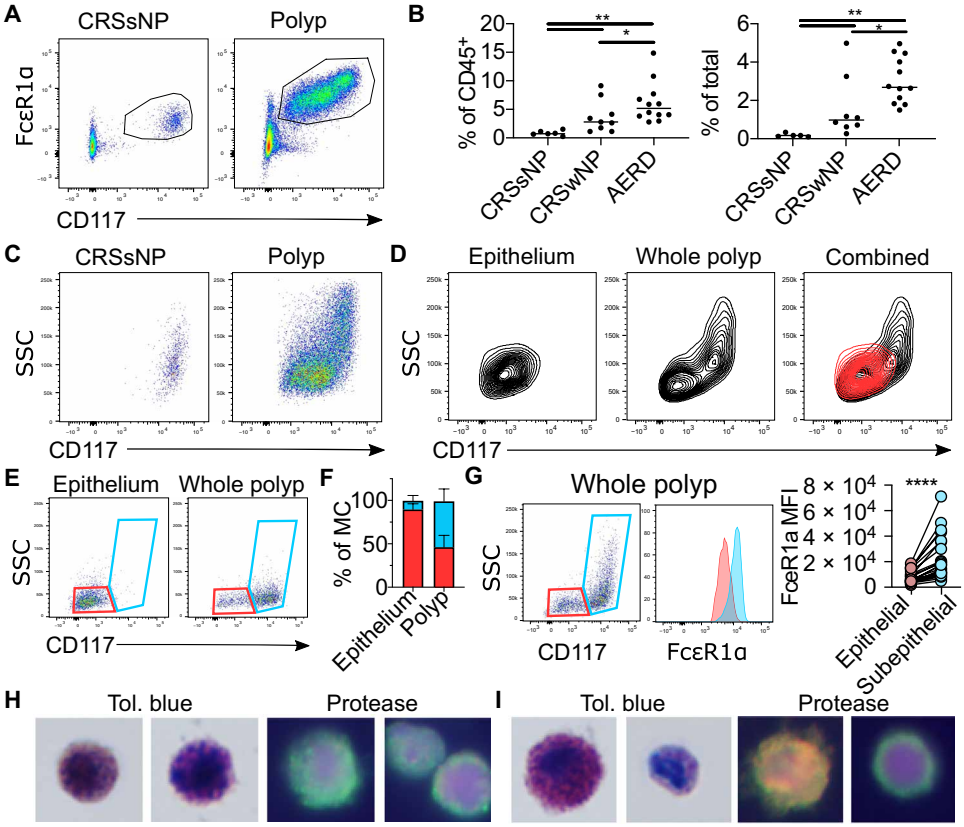

Fig. 1. Phenotypic characterization of sinus MC hyperplasia. (**A**) Flow identification of human sinus MCs. (Additional replicates and full gating in fig. S1). (**B**) MC quantification as percentage of CD45$^+$ (left) or total cells (right) in indicated patient groups ($n = 6$ to 12 donors per group). *$P < 0.05$ and **$P < 0.01$ (Mann-Whitney). (**C**) Representative plots showing MC heterogeneity in nasal polyp (left) or CRSsNP tissue (right). (**D**) MC phenotype in polyp epithelium (left), whole polyp (center) with overlay (right). Red, epithelium; black, whole polyp. Representative of five donors. (**E**) Gating distinguishing epithelial MCs (CD117^{low} SSC^{low}, red) from subepithelial MCs (CD117^{high}, blue) in epithelial fraction (left) versus unfractionated polyp (right). (**F**) Quantification of epithelial and subepithelial MCs in fractionated epithelium and unfractionated polyp ($n = 5$ donors); *$P < 0.05$ (paired t test). (**G**) FcεR1α expression of epithelial (red) and subepithelial MCs (blue) with quantification (right). Lines denote paired observations ($n = 24$ donors); ****$P < 5 \times 10^{-5}$ (paired t test). MFI, mean fluorescence intensity. (**H**) Toluidine blue (left) and protease immunophenotyping (right) of sorted CD117^{low} MCs. Two examples are provided to show heterogeneity. Green, tryptase; red, chymase; yellow, colocalization; blue, nucleus. (**I**) Toluidine blue (left) and protease immunophenotyping (right) of CD117^{high} MCs. Two examples are provided to show heterogeneity. Green, tryptase; red, chymase; yellow, colocalization; blue, nucleus.

absent in CRSsNP tissue (Fig. 2C) and present in similar concentrations in CRSwNP and AERD relative to total MCs (Fig. 2D). Unlike circulating MCp, Itgβ7^{high} MCs were CD34$^-$ (Fig. 2E). Itgβ7 pairs with the integrins αE and α4, forming either αEβ7, recognizing the epithelial adhesion molecule E-cadherin, or α4β7, recognizing vascular cell adhesion molecule and mucosal addressin cell adhesion molecule 1 (*25*, *26*). Although circulating Itgβ7^{high} MC$_P$ expressed only α4, a substantial subset of polyp Itgβ7^{high} MCs coexpressed αE (Fig. 2F). These αE^{high} MCs were mostly in the epithelial-enriched CD117^{low} gate, whereas Itgβ7^{high} cells lacking αE were not significantly enriched in either compartment (Fig. 2G). Thus, Itgβ7^{high} polyp MCs are a heterogeneous population distinguished from circulating MC$_P$ by lack of CD34 expression, increased granulation, and expression of αE integrin, together likely reflecting maturation in response to the tissue microenvironment. As αEβ7 binds epithelial-associated E-cadherin (*25*), its expression could promote accumulation or retention in the epithelial compartment.

scRNA-seq identification of MC polarization and proliferation

To further explore polyp MC heterogeneity, we conducted scRNA-seq using the Seq-Well platform on MCs flow sorted from six polyp donors (Fig. 3A) (*27*). We derived a unified cell-by-gene matrix for all cells passing quality control thresholds (n = 7355 cells) and identified 10 cell clusters after dimensionality reduction and unsupervised clustering (fig. S3A and Materials and Methods). Contaminating populations were identified by comparison to a series of cell-identity transcriptional signatures developed in our prior scRNA-seq study of nasal polyposis (*22*), including small populations of fibroblasts and epithelial cells, DCs, B/plasma cells, and a population of plasmacytoid DCs (pDCs) not resolved in our previous study (fig. S3, B to E, and tables S2 and S3). All clusters were observed in CRSwNP and AERD and in all patients aside from one lacking pDCs (fig. S3F). The consistent presence of these contaminating cells within the sorted MC pool from six donors indicates the necessity of including additional markers to identify human MCs under conditions where contaminating populations cannot be computationally removed, such as bulk RNA-seq or functional assays. The four remaining clusters, designated as MC1 to MC4 (Fig. 3B), all strongly expressed the MC proteases tryptase (*TPSAB1*) and CPA3 (*CPA3*) and similar levels of transcripts encoding the histamine biosynthetic enzyme histidine decarboxylase (*HDC*) and the lipid mediator biosynthetic enzymes prostaglandin D_2 synthase (*HPGDS*), 5-lipoxygenase (*ALOX5*), and 5-lipoxygenase activating protein (*ALOX5AP*) (Fig. 3C). The MC1 to MC3 clusters further showed similar expression of a set of core transcripts highly enriched in nasal polyp MCs (*22*), including the MC granule core protein serglycin (*SRGN*) and the transcription factor GATA2 (*GATA2*) (Fig. 3D, top). Together, these observations indicated that MCs within the polyp environment share a core effector program enabling the generation of proteases, lipid mediators, and histamine.

Differential gene expression analysis between the four identified MC clusters indicated MC1-enriched expression of chymase (*CMA1*) and cathepsin G (*CTSG*) (Fig. 3D), consistent with subepithelial MC$_{TC}$ (Fig. 1I and fig. S2). The MC2 cluster lacked enriched genes, whereas the MC3 cluster expressed minimal *CMA1* and *CTSG* and reduced levels of transcripts encoding both CD117 (*KIT*) and the high-affinity IgE receptor FcεR1α (*FCER1A*) compared with the MC1 cluster, consistent with epithelial MC$_T$ (Figs. 3D and 1H). The MC3 cluster was additionally enriched for *IL17RB*, encoding the receptor

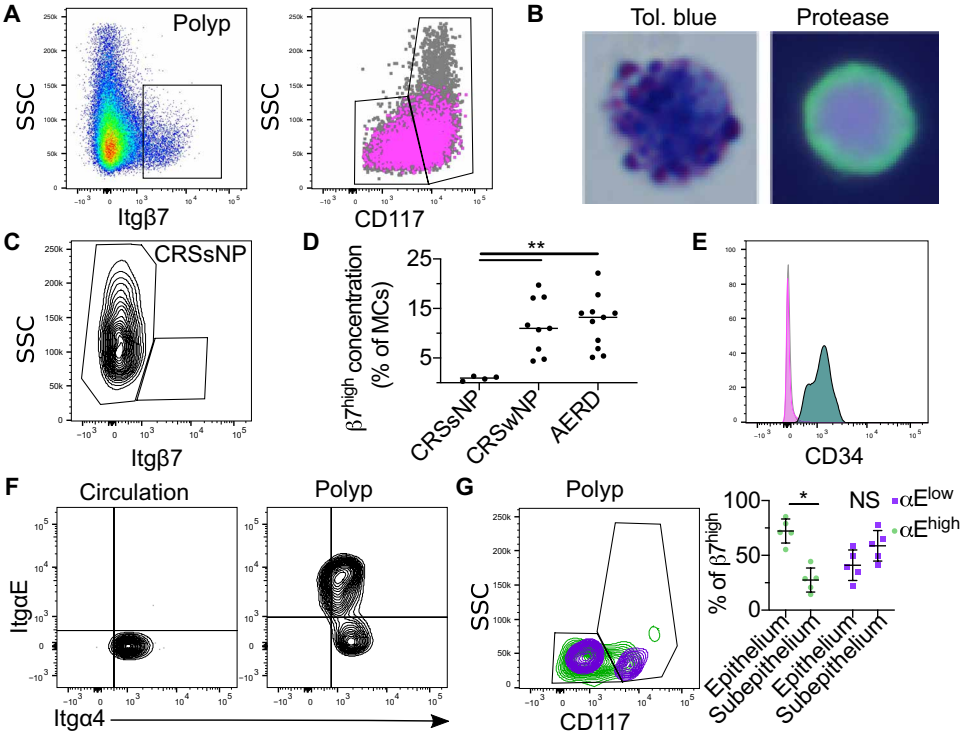

Fig. 2. Identification polyp MCs with a progenitor-like cell surface phenotype. (**A**) Identification of nasal polyps SSC^{low}Itgβ7^{high} MCs (left). CD117 and SSC expression on Itgβ7^{high} MC (magenta) relative to all polyp MCs (gray) (right). (**B**) Toluidine blue (left) and protease immunophenotype (right) of sorted Itgβ7^{high} polyp MCs MCs. Green, tryptase; red, chymase; blue, nucleus. (**C**) Representative flow plot of Itgβ7 expression on CRSsNP MCs. (**D**) Quantification of Itgβ7^{high} MCs as a percentage of total MCs in CRSsNP, CRSwNP, and AERD. $^{**}P < 0.01$ (Mann-Whitney). (**E**) CD34 expression on polyp Itgβ7^{high} MCs (magenta) and circulating MC$_P$ (turquoise) versus isotype (gray), representative of three independent donors (magenta and gray are superimposed). (**F**) Integrin expression on circulating MC$_P$ (left) and polyp Itgβ7^{high} MCs (right), each representative of three separate donors. (**G**) Distribution of polyp αE^{high} (green) and αE^{-} (purple) Itgβ7^{high}MCs distribution within the epithelial versus subepithelial gates (left) as in Fig. 1E, with quantification (right). $^{*}P < 0.05$ (paired *t* test).

for the epithelial-associated cytokine interleukin-25 (IL-25), and *GPR183*, encoding the chemotactic receptor Epstein-barr virus-induced G-protein coupled receptor 2 (EBI2) (*28*, *29*). Immunofluorescence confirmed colocalization of tryptase and EBI2 within the epithelium, although not all MCs within the epithelium expressed detectable EBI2 (fig. S4). Unexpectedly, the MC4 cluster expressed transcripts involved in proliferation and DNA replication, including *TOP2A* (encoding DNA topoisomerase IIA) and *MKI67* (encoding the cell cycle phase–associated protein KI67) (Fig. 3D and table S4).

We further observed that the transcriptional signatures associated with MC1 and MC3 (table S4) were expressed along gradients (Fig. 3E). These cluster-defining signatures exhibited negative correlation on a per-cell basis, with the MC2 cluster expressing low levels of each, suggesting an intermediate state (Fig. 3F, top). Cells within the proliferative cluster showed a range of MC1 and MC3 signature expression similar to that seen in the MC2 cluster, and the MC1 and MC3 signatures were again negatively correlated on a per-cell basis (Fig. 3F, bottom). This suggested that the polyp MC$_{TC}$ (MC1) and MC$_T$ (MC3) transcriptional programs represented polarization states layered on a common shared transcriptome and that the proliferative population (MC4) shared transcriptional overlap with unpolarized MCs (MC2).

To better understand the transcriptional differences between the two polarized MC states, we directly compared the MC1 (MC$_{TC}$) cluster to the MC3 (MC$_T$) cluster. These populations exhibited differential expression of 282 transcripts (Wilcoxon, $P_{adj} < 0.05$) (Fig. 3G and table S4). The MC1 (MC$_{TC}$) cluster showed enhanced expression of chemokines (*CCL2*, *CCL3*, *CCL4*, and *CKLF*), myeloid cell growth factors (*CSF1* and *CSF2*), the cytokine *IL13*, and the lipid mediator biosynthetic enzyme *PTGS2* (Fig. 3H), suggesting that they are poised to coordinate proinflammatory responses through several mechanisms. Although all MC clusters expressed transcript encoding the protease CPA3 (Fig. 3C), this was enriched within MC3 (MC$_T$) cluster (Fig. 3G). MC3 additionally showed enhanced expression of *TNFSF10*, encoding TNF-related apoptosis-inducing ligand (TRAIL), which positively regulates airway inflammation and remodeling in murine models of asthma (*30*, *31*), *FGL2*, which shifts DC and T cell interactions toward T helper cell 2 (T$_H$2) polarization (*32*) (Fig. 3H), and *IL17RB* (Fig. 3G), suggesting the potential for this population to modulate T2-driven responses within the epithelium and respond to epithelial-derived IL-25.

Previous studies have indicated that epithelial-derived factors inhibit IgE-dependent MC activation (*33*, *34*). Accordingly, the MC$_T$ cluster showed reduced expression of components of the FcεR1 complex (*FCER1A*, *MS4A2*, and *FCER1G*) and the downstream regulator *BTK* (Fig. 3I). In contrast, no significant difference was observed for expression of the IL-33 receptor *IL1RL1* (table S4). To test whether activation states of polyp MC$_{TC}$ and MC$_T$ differed more broadly, we constructed MC activation transcriptional signatures based on existing microarray datasets evaluating murine bone marrow–derived MC activation (table S2) (*35*). We found that MC1 (MC$_{TC}$) expressed the highest levels of transcript signatures specific to IgE-mediated activation, specific to IL-33–mediated activation, and commonly up-regulated by both signals, whereas the MC3 (MC$_T$) exhibited decreased expression and MC2 expressed intermediate levels (Mann-Whitney, $P < 1 \times 10^{-11}$ for all comparisons) (Fig. 3J). Thus, polyp MC$_{TC}$s are activated at baseline, reflected in their increased cytokine and chemokine expression, and the intermediate MC2 exhibit activation despite a lack of polarization.

Identification of a distinct MC$_T$ phenotype associated with respiratory tract inflammation

Several genes identified as part of the MC$_T$ transcriptome, including *GPR183*, *IL17RB*, and *CD38*, were not previously associated with human MCs. To determine whether this phenotype was restricted to nasal polyposis or associated with broader inflammatory conditions, we evaluated three lung scRNA-seq datasets from patients with fibrosis included within the idiopathic pulmonary fibrosis (IPF) cell

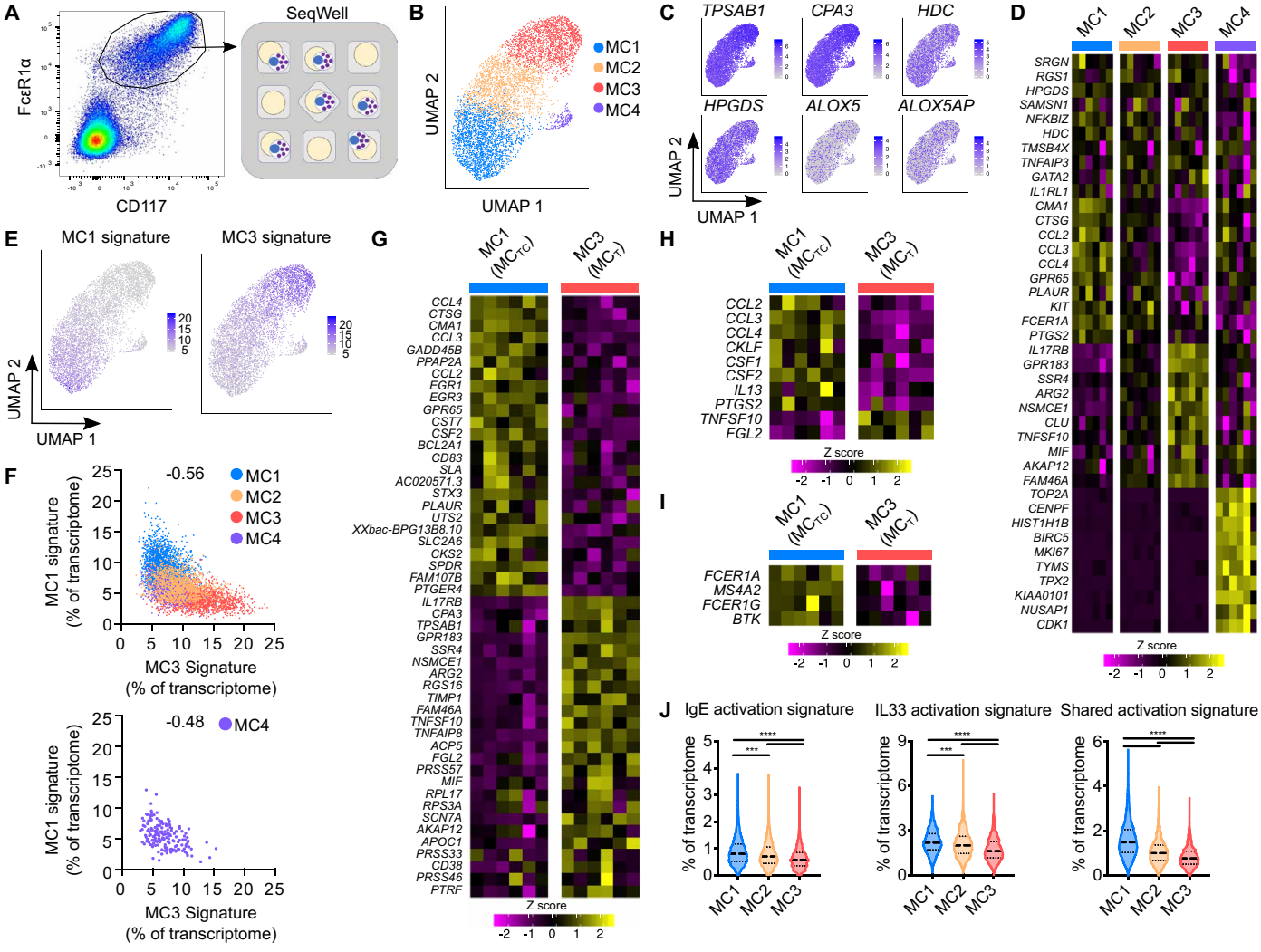

Fig. 3. scRNA-seq identification of transcriptionally distinct polyp MC subsets. (**A**) Schematic representation for scRNA-seq analysis of 7355 cells sorted polyp MCs (fig. S1) ($n = 6$ donors). (**B**) UMAP depiction of MC clusters (fig. S3 depicts identification of MC versus contaminating clusters). (**C**) MC expression of canonical MC transcripts. (**D**) Common (top rows) and cluster-enriched transcripts (columns show donor-averaged row-normalized expression). $P_{adj} < 3.1 \times 10^{-29}$ for cluster-enriched genes (Wilcoxon). (**E**) Polyp MC expression of MC1 and MC3 signatures (% of transcripts per cell). (**F**) Per-cell expression of MC1 and MC3 signatures across all clusters (top) and MC4 alone (bottom) (correlation r value). (**G**) Differentially expressed transcripts between polyp MC_{TC} (MC1) and MC_T (MC3), (donor averaged and row normalized); $P_{adj} < 6 \times 10^{-9}$ (Wilcoxon). (**H**) Immunomodulatory transcript expression in polyp MC_{TC} and MC_T, (donor averaged and row normalized); $P_{adj} < 7 \times 10^{-17}$ (Wilcoxon). (**I**) FcεR1 signaling pathway expression in polyp MC_{TC} and MC_{TC} (donor averaged and row normalized); $P_{adj} < 8 \times 10^{-4}$ (Wilcoxon). (**J**) Expression of transcript scores driven by IgE signaling, IL-33 signaling, or shared by both stimuli across the MC1 to MC3 clusters (lines denote median and quartiles). ****$P < 1 \times 10^{-10}$ and ***$P < 1 \times 10^{-15}$ (Mann-Whitney); Cohen's effect size for MC1 versus MC3: 0.60 (IgE), 0.79 (IL-33), and 1.52 (shared).

atlas (*36*). These datasets included analyses of IPF and interstitial lung disease (ILD) versus healthy control (*37*), IPF and chronic obstructive pulmonary disease (COPD) versus healthy control (*38*), and IPF versus healthy control (*39*). Prior studies have found increased expression of transcripts encoding the T2 cytokine signaling pathway and the MC protease *CPA3* in IPF (*40*). Independent analysis of each of the three datasets identified a prominent *TPSAB1*-expressing MC cluster (fig. S5). MCs from each dataset were separately reclustered, and substantial disease-associated MC heterogeneity was noted within each (Fig. 4, A to C, left; and table S5). We observed a cluster of MCs within each dataset exhibiting significant enrichment for *CD38*, *GPR183*, and *IL17RB* (Fig. 4, A to C, middle, polygon gate) and further noted MCs coexpressing the proliferation-associated genes *MKI67* and *TOP2A* in two of the three datasets (Fig. 4, A to C, middle, circle gate). Across each dataset, the $CD38^{high}$ populations consisted predominantly of MCs from IPF or ILD (Fig. 4, A to C, left). We further identified an MC cluster significantly enriched for both *CD38* and *CPA3* (fig. S6A, cluster outlined in black) in a reanalysis of a prior scRNA-seq study of lung biopsy samples from asthmatic versus controls (*41*) in which *IL17RB* and *GPR183* expression could also be observed although neither reached statistical significance (fig. S6B and table S5). A comparison of genes significantly enriched within the $CD38^{high}$ clusters across the three fibrosis datasets identified substantial transcriptional overlap, with 18 transcripts enriched in all three datasets, including *CPA3*, and 85 transcripts enriched within the $CD38^{high}$ cluster in at least

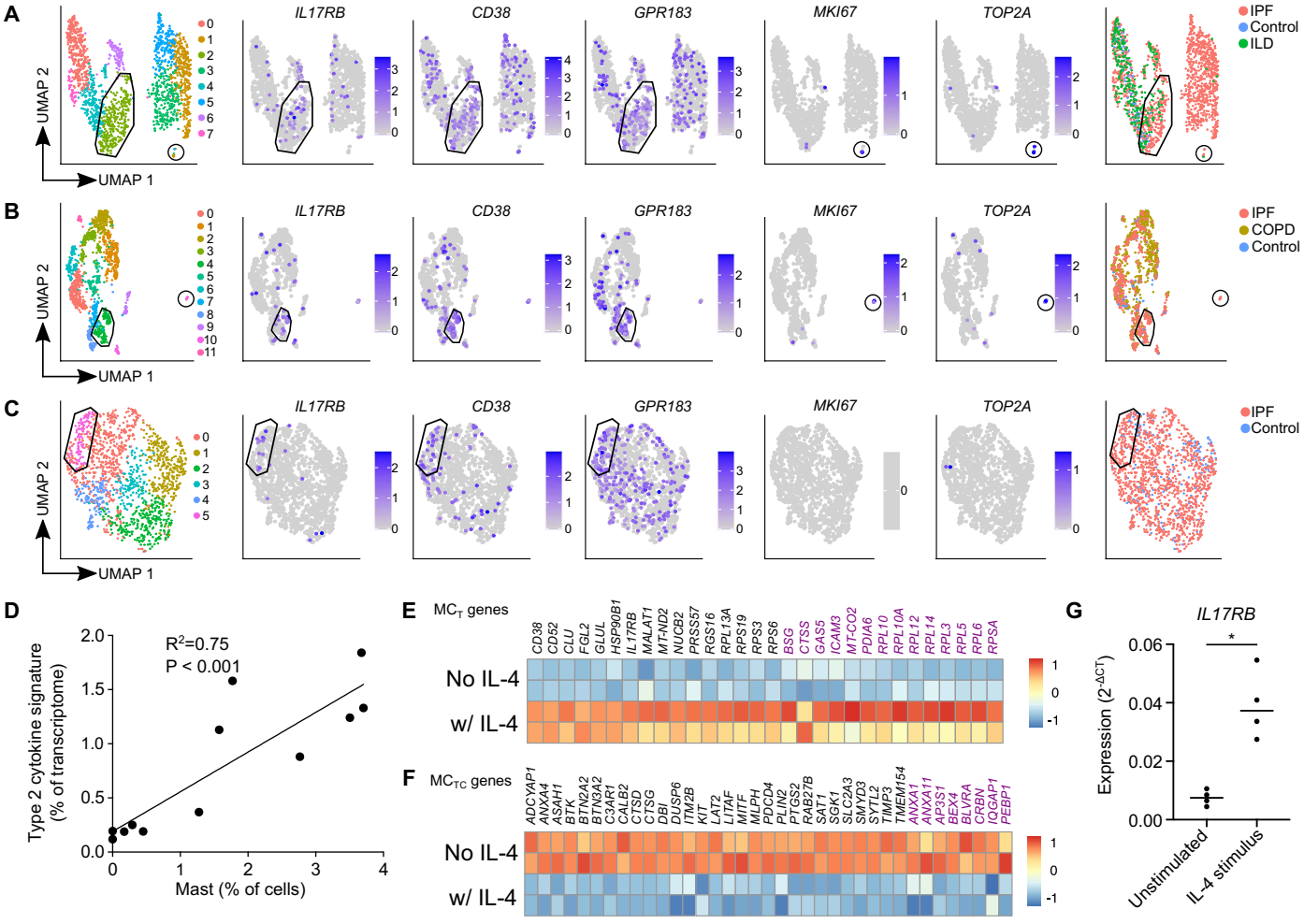

Fig. 4. Characterization of an IL-4–elicited MC_T phenotype enriched in diseased human lung samples. (**A** to **C**) Reclustering of MCs from three scRNA-seq datasets accessed through the human IPF atlas: (A) control, IPF, and ILD; (B) control, IPF, and COPD; and (C) control and IPF. Clustering for each dataset indicated a population (polygon gate) that was statistically enriched for the polyp MC3-associated transcripts *IL17RB*, *CD38*, and *GPR183* (middle) and predominantly composed of MCs from diseased tissue relative to healthy (left). Circle gate indicates MCs coexpressing the proliferation-associated genes *MKI67* and *TOP2A*. (**D**) Correlation analysis of polyp scRNA-seq epithelial IL-4/13–induced signature expression, (donor averaged) versus scRNA-seq–defined MC percentage for each donor. $P < 0.001$. (**E**) MC3-enriched transcripts (table S4) up-regulated in two technical replicate CBMC samples by 96-hour IL-4 stimulus (row-normalized expression). Top half: False discovery rate (FDR) < 0.1, bottom half (indicated by purple line): $P < 0.05$ (DESeq2). (**F**) MC1-enriched transcripts (table S4) down-regulated in two technical replicate CBMC samples by 96-hour IL-4 stimulus (row-normalized expression). Top half: FDR < 0.1 and bottom half (indicated by purple line): $P < 0.05$ (DESeq2). (**G**) CBMCs *IL17RB* expression (qPCR) after 72-hour stimulus with vehicle or IL-4, ($n = 4$ biologic replicates across three independent experiments), * indicates $P < 0.05$ (paired *t* test).

two of the three datasets (Wilcoxon, $P < 0.05$; Table 1). These transcripts overlapped with transcripts enhanced in both polyp MC_T (19 transcripts) and the *CD38*-enriched asthma-associated cluster (38 transcripts), indicating a common inflammation-associated transcriptional program.

Expression of *IL17RB* by MCs in the lungs of patients with fibrosis and asthma and CRSwNP polyps suggested that this transcript was regulated by disease-associated signals. Mouse studies have identified a central role for IL-4 in intraepithelial MC expansion (*42*, *43*), and a reanalysis of our prior nasal polyposis scRNA-seq dataset indicated a significant correlation between polyp MC concentration and epithelial expression of an IL-4/IL-13–driven cytokine signature (Fig. 4D) (*22*). *IL4* expression in nasal polyposis was restricted to T_H2A cells, whereas *IL13* was expressed by both T_H2A cells and MCs (*22*). Further, reanalysis of scRNA-seq data from a single CRSwNP donor evaluated before and after 6 weeks of treatment with dupilumab, a monoclonal antibody directed against the IL-4 receptor, revealed markedly reduced *IL17RB* expression within the MC cluster compared with pretreatment baseline but no change in expression of the MC_T-associated transcript *GPR183* (fig. S7). Thus, we hypothesized that IL-4 directly influenced polyp MC_Ts.

To evaluate IL-4 regulation of the polyp MC_T transcriptome, human cord blood–derived MCs (CBMC) were stimulated with IL-4 or vehicle for 96 hours and then analyzed via RNA-seq. IL-4 exerted a profound impact on the CBMC transcriptome (table S6). Among the up-regulated genes were 30 of 102 polyp MC_T–enriched transcripts, including *IL17RB* and *CD38* but not *GPR183* (Fig. 4E and table S6). IL-4 conditioning also down-regulated 37 of 180 MC_{TC}-enriched transcripts, including *CTSG* and *KIT* (Fig. 4F). The capacity for IL-4 to up-regulate *IL17RB* was further confirmed

through quantitative polymerase chain reaction (qPCR) analysis (Fig. 4G). However, IL-4 stimulus also up-regulated FcεR1 signaling components (table S6) that were down-regulated in polyp MC_T (Fig. 3I), suggesting that other signals additionally regulate the MC_T transcriptome. Thus, our findings identified a distinct phenotype of MC_T associated with respiratory inflammation and identified the potential for IL-4 signaling to regulate this phenotype.

Recognition of MC_{TC} heterogeneity across tissues

Although chymase-expressing MCs found in mucosal tissues during inflammation are termed as MC_{TC}, the relatedness of these cells to constitutive MC_{TC} populations present in peripheral tissues such as the skin has not been addressed. Thus, we compared nasal polyp MCs to dermal MCs derived from a scRNA-seq study of healthy and diseased human skin biopsies from patients with psoriasis, alopecia, acne, leprosy, and granuloma annulare (*44*). Polyp MC1 (MC_{TC}) and dermal MCs, canonically exhibiting an MC_{TC} phenotype (*5*), both showed enhanced expression of *CMA1* relative to polyp MC1 (MC_T), as well as a shared subset of receptors (*KIT*, *PLAUR*, and *ICAM1*) and mediators (*LIF* and *CSF1*) (Fig. 5A). However, dermal MC_{TC} lacked expression of other transcripts strongly expressed in polyp MCs and vice versa. Polyp MC1s (MC_{TC}) were enriched in expression of chemokines (*CCL2*, *CCL3*, and *CCL4*) and FcεR1α signaling pathway transcripts (*FCER1A*, *MS4A2*, and *BTK*) relative to dermal MCs but lacked expression of genes encoding the activating G protein–coupled receptors CD88 (*C5AR1*) and Mas-related G-protein coupled receptor X2 (*MRGPRX2*), previously described as markers for MC_{TC} in the skin and lung (*45*, *46*). Supporting this observation, we found strong surface expression of MRGPRX2 on skin-derived MCs but little to no expression on polyp MCs (Fig. 5B). To determine whether the absence of these receptors reflected the polyp inflammatory environment a broader paradigm of MC_{TC} heterogeneity, we conducted an independent analysis of an existing scRNA-seq dataset containing distal (alveolar), medial, and proximal (large bronchi) fractions of healthy lung developed by Travaglini *et al.* (*47*). After normalization, we identified a prominent *TPSAB1*-expressing MC cluster (Fig. 5C). Despite the presence of similar numbers of MCs expressing *CMA1* and *CTSG* in the distal and proximal lung, *MRGPRX2* expression could only be detected in the large airway (Fig. 5D). Although not reaching statistical significance, this observation suggests that MC_{TC} exhibit heterogeneity even within a single tissue. *C5AR1*, encoding CD88, was only weakly detected in either lung compartment. These findings indicate considerable differences in the transcriptome of chymase-expressing MCs across tissues and inflammatory milieus and further highlight the activated state of polyp MCs and their likely pathogenic contributions. Moreover, the findings further illustrate the vast extent of MC heterogeneity that is not reflected by conventional histochemical criteria.

Identification of CD117 and CD38 cell surface expression patterns defining polyp MC phenotypes

Among the transcripts enriched in MC3 (MC_T) relative to MC1 (MC_{TC}) clusters was *CD38* (Fig. 3G), suggesting a candidate cell surface marker that might further distinguish polyp MC subsets. Cell surface staining indicated virtually all $CD117^{low}$ epithelial MC_Ts exhibited high CD38 expression (Fig. 6, A and B; red gate). Unexpectedly, CD38 expression also divided the heterogeneous $CD117^{high}$ subepithelial MC pool (Fig. 1C) into $CD38^{high}SSC^{low}$ MCs (orange) and $CD38^{neg}$ MCs with a range of SSC (blue). $Itg\beta7^{high}$ polyp MCs expressed CD38 (Fig. 6C). A subset of cells lacking both CD117 and CD38 (Fig. 6A) was likely the source of contaminants observed through scRNA-seq (fig. S3). $CD38^{high}CD117^{high}$ subepithelial MCs were also detected in CRSsNP tissue; however, their relative abundance was significantly reduced when compared with CRSwNP and AERD polyps (Fig. 6, D and E). No significant differences were observed in MC subset composition between CRSwNP and AERD. Thus, CD38 marks polyp epithelial MC_T and Itgβ7-expressing MC, as well as a $CD117^{high}$ subepithelial MC subset significantly expanded in nasal polyps.

Enriched CD38 expression in $CD117^{low}$ MCs (Fig. 6A) and reduced *CD38* in MC1 relative to MC3 (Fig. 3G) suggested that $CD117^{high}CD38^{low}$ subepithelial MCs were mature MC_{TC}. Flow cytometry confirmed that $CD117^{low}$ intraepithelial MCs (red) lacked chymase expression (Fig. 6F), consistent with immunofluorescent staining (Fig. 1H), whereas subepithelial $CD117^{high}CD38^{low}$ MCs (blue) were uniformly positive for chymase, indicating an MC_{TC} phenotype (Fig. 6, F and G). The $CD38^{high}CD117^{high}$ MC gate included both chymase-positive and chymase-negative cells (Fig. 6F). Similarly, staining with avidin, a reagent that binds to heparin sulfate (*48*) and specifically identifies human MC_{TC} (*49*), was highest in subepithelial $CD117^{high}CD38^{low}$ MC_{TC} (blue), lowest in $CD117^{low}CD38^{high}$ (red) epithelial MC_T, and intermediate in $CD117^{high}CD38^{high}$ MCs (yellow) (Fig. 6, H and I). Thus, through surface marker expression and intracellular protease and heparin staining, we could identify mature intraepithelial MC_T ($CD117^{low}$ $CD38^{high}$; red) and subepithelial MC_{TC} ($CD117^{high}CD38^{low}$, blue) and further identify a subepithelial population with an intermediate phenotype ($CD117^{high}CD38^{high}$, yellow), suggestive of the MC2 subset identified through scRNA-seq.

Evaluation of in situ proliferation within human polyp MCs

To integrate our transcriptional analysis with these flow cytometrically defined MC subsets, we used CITE-seq (*50*) to simultaneously assesses RNA and surface protein expression on flow-sorted polyp MCs, using oligo-tagged antibodies directed against CD117, CD38, and Itgβ7 (Fig. 7A). Clustering again identified the same four MC populations (Fig. 7B and table S4), indicating that MC_{TC} (MC1) exhibited high surface CD117 and low surface CD38, whereas MC_T (MC3) exhibited low surface CD117 and high surface CD38 (Fig. 7C). We further observed that the MC2 cluster exhibited intermediate surface CD117 and CD38 levels, confirming its identity as the flow cytometrically defined $CD38^{high}CD117^{high}$ population, and that the proliferating MC4 seen similarly exhibited elevated CD38 and CD117 levels. Surface Itgβ7 was predominantly observed in the MC3 cluster (Fig. 7D), in agreement with the previously observed epithelial enrichment of $Itg\alpha E^{+}\beta7^{+}$ MCs (Fig. 2G), but scattered Itgβ7 expression was also observed across all clusters. A direct comparison of $Itg\beta7^{high}$ and $Itg\beta7^{low}$ MCs within each cluster indicated little to no impact of Itgβ7 expression on the MC transcriptome (fig. S8).

Our CITE-seq observations suggested that the majority of proliferating MCs would be $CD117^{high}CD38^{high}$ subepithelial MCs. Nuclear KI67 staining identified a distinct population of proliferating MCs (Fig. 7E), and whereas proliferation was observed across all three compartments, the majority of $Ki67^{+}$ cells were $CD117^{high}CD38^{high}$ subepithelial MCs (Fig. 7F). Combined with the detection of both MC_T and MC_{TC}-associated transcript signatures within the proliferating clusters detected through scRNA-seq (Fig. 3F), these

Table 1. Identification of inflammation-associated airway MC_T transcripts across datasets. Transcripts significantly elevated in *CD38*, *IL17RB*, and *GPR183*-enriched MCs ($P < 0.05$) in at least two of the three lung fibrosis scRNA-seq datasets analyzed. Transcripts in bold were significantly elevated in polyp MC3 (MC_T) relative to other polyp subsets. Blue transcripts were significantly elevated within the CD38-enriched asthma MC cluster analyzed in fig. S6.

Banovich and Kropski	+	+	+	–
Kaminski and Rosas	+	+	–	+
Lafayatis	+	–	+	+
	ACTG1	*ABRACL*	*B4GALT5*	***AKAP12***
	CD38	*ACTR3*	*BCL2A1*	*ARHGEF6*
	CD52	*CAPG*	***CALR***	*CELF2*
	CPA3	*EEF1G*	*CAMK1*	*EEF2*
	CXCR4	*EIF2A*	*CD83*	*FBXO34*
	DTNBP1	*HOTAIRM1*	*CDC42*	*LCP2*
	EEF1A1	*LTC4S*	*CKS2*	*NEDD9*
	GPR183	*MYL12B*	*CREM*	*PLXNC1*
	IL17RB	*NKG7*	*DUSP10*	*PROM1*
	LDLRAD4	***RPL10A***	*DUSP4*	*RPL28*
	LGALS1	***RPL13A***	*EHD1*	*RPLP0*
	MAFF	*RPL15*	*FOSL2*	*SLC9A1*
	NSMCE1	***RPL3***	*GALNT6*	
	PFN1	*RPL7*	*GEM*	
	RGS16	*RPS2*	*HES4*	
	RPL4	*RPS5*	*HEY1*	
	RPSA	***RPS6***	***ICAM3***	
	ZC3H12A	*RPS9*	*ID2*	
		SVOPL	*ISG15*	
		TMSB4X	*KDM6B*	
		TPI1	*KPNA2*	
		TPSAB1	*LMNB1*	
		UQCRH	*MAT2A*	
			MCL1	
			NFATC1	
			NR4A1	
			NR4A2	
			NR4A3	
			NUDT14	
			PHLDA1	
			PLAUR	
			PMEPA1	
			PRKD3	
			PTGS2	
			RAB33A	
			RANBP2	
			SETP9	
			RUNX3	
			SH2D2A	
			SKIL	
			SLC16A3	
			SRSF2	
			TGIF1	
			TNFAIP8	
			TNFRSF9	
			TPM4	
			TPT1	
			ZFAND5	
			ZNF331	

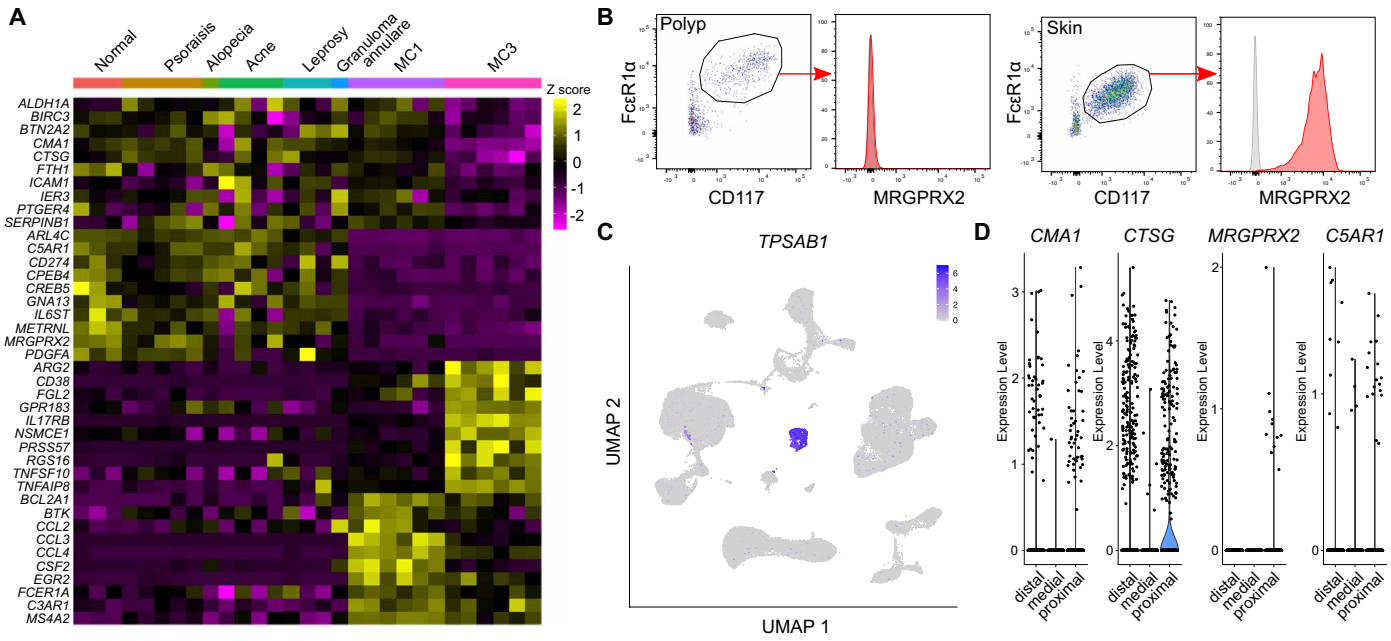

Fig. 5. Identification of MC_{TC} heterogeneity across tissues. (**A**) Transcripts shared between diseased and control skin MCs and polyp MC_{TC} (top) versus enriched in skin MCs (top middle), polyp MC_T (bottom middle), or polyp MC_{TC} (bottom) (donor averaged and row normalized). (**B**) Representative analysis of MRGPRX2 expression (red) on nasal poly MCs (left) and skin MCs (right) relative to isotype (gray). Staining representative of three donors per group. (**C**) Identification of MCs based on expression of tryptase (TPSAB1) within an scRNA-seq dataset of healthy human lung tissue containing samples from distal, medial, and proximal lung generated by Travaglini *et al.* (*47*). (**D**) Violin plots showing expression of the MC_{TC}-associated transcripts *CMA1*, *CTSG*, *MRGPRX2*, and *C5AR1* in healthy human lung. No displayed transcripts were significantly differentially expressed between distal and proximal lung; MRGPRX2 expression was only observed in proximal lung.

findings suggest that the MC hyperplasia characteristic of human nasal polyposis is driven, in part, by in situ MC proliferation. Consistent with this hypothesis, we observed a significant increase in MC proliferation in the polyps of patients with AERD relative to MC from CRSwNP donors (Fig. 7G), corresponding to the differences in polyp MC concentration between these two patient groups (Fig. 1B). We further noted a significant correlation between MC proliferation and peripheral blood eosinophilia across all patients with polyps (Fig. 7H), indicating a link between MC proliferation and overall disease severity. Coupled with the previous observation that progenitor-like Itgβ7-expressing MCs were present at similar concentrations in AERD and CRSwNP (Fig. 2D), our findings suggest an important role for local proliferation in MC hyperplasia during T2 airway inflammation.

DISCUSSION

Our study provides a transcriptomic and flow cytometric characterization of MC hyperplasia during human airway inflammation, identifying proliferation as a driver of T2-associated nonneoplastic MC airway hyperplasia. We also observe that MC sensing and effector programs are closely linked to tissue microenvironments. The MC_T and MC_{TC} phenotypes in CRSwNP tissue display substantial cell surface differences and predominate in epithelial and subepithelial regions, respectively. Despite shared expression of a core transcriptome, they inhabit opposite poles of a transcriptional gradient, implying distinct functions for each. The CRSwNP MC_T program, distinguished by expression of *CD38*, *IL17RB*, and *GPR183*, is also observed within the lungs of IPF, ILD, and asthma patients. These MC_Ts further express elevated *CPA3*, suggesting a link to the $CPA3^+$ MC_Ts previously reported in the bronchial epithelium of asthmatics and esophagus of patients with EoE (*15*–*18*). The CRSwNP MC_{TC} program, enriched for proinflammatory cytokines and chemokines, differs from classical skin and noninflamed lung MC_{TC}s by its lack of the MC_{TC} markers MRGPRX2 and CD88 (*C5AR1*) (*45*, *51*, *52*). Both MC_T and MC_{TC} populations expand markedly in CRSwNP tissue and even more so in AERD tissue, relative to CRSsNP controls. On the basis of these observations, we propose that these expanded mucosal T2 inflammation–associated MC subsets be reclassified as airway inflammatory MC_T and MC_{TC} (iMC_T and iMC_{TC}), respectively, distinguishing them from their counterparts in nonmucosal tissues and tissues with less T2 inflammation (fig. S9).

The stark transcriptional differences between iMC_T and iMC_{TC} imply both distinct functions and distinct patterns of imprinting by tissue-associated factors. Both iMC_{TC} and transitional MC clusters display enrichment for FcεRI-inducible and IL-33–inducible transcripts characterized by chemokines (*CCL2*, *CCL3*, and *CCL4*), cytokines (*IL13*), growth factors (*CSF1* and *CSF2*), and *PTGS2* [encoding cyclooxygenase-2, required for prostaglandin D_2 (PGD_2) generation]. Thus, subepithelial MCs may respond to both innate (IL-33) and adaptive (IgE) immune pathways to provide mediators driving recruitment and activation of blood-born effector cells and conditioning the surrounding stroma. Although iMC_T display lower levels of activation-associated transcripts, they uniquely express *IL17RB*, the receptor for the epithelial-derived T2 cytokine IL-25. *IL17RB* is also expressed by MCs in the lungs of IPF, ILD, and patients with asthma, indicating that it is part of a disease-associated human

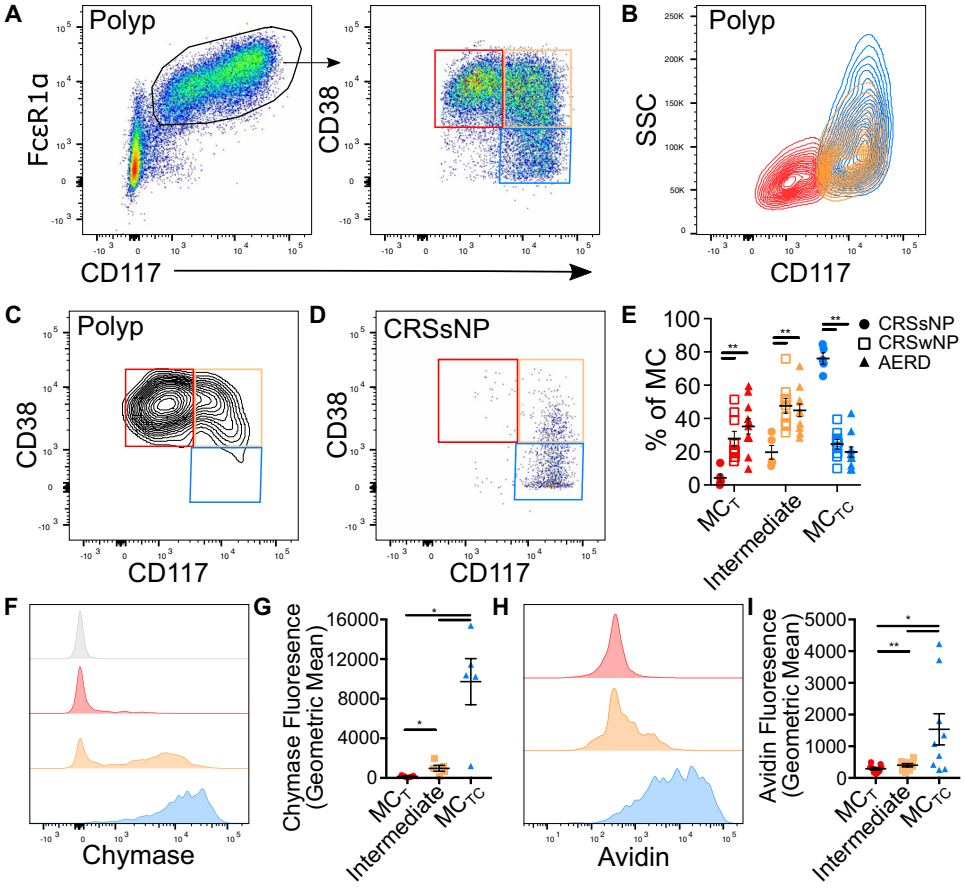

Fig. 6. CD38 expression marks nasal polyp MC_T and an unpolarized intermediary subset. (**A**) Representative plot showing nasal polyp MC (gated as in fig. S1) expression of CD38 and CD117. Arrow indicates sequential gating. (**B**) SSC versus CD117 profile of $CD38^{high}$ epithelial MCs (red), $CD38^{high}$ subepithelial MCs (orange), and $CD38^{low}$ subepithelial MCs (blue). (**C**) Representative plot showing CD38 and CD117 expression in $Itg\beta7^{high}$ MCs. (**D**) Representative plot of MC CD38 and CD117 expression in CRSsNP control tissue. (**E**) Quantification of $CD38^{high}CD117^{low}$ MC_T (red), $CD38^{high}CD117^{high}$ intermediate MCs (orange), and $CD38^{low}CD117^{high}$ MC_{TC} (blue) in sinus tissue of patients with CRSsNP (closed circles), CRSwNP (open squares), or AERD (closed triangles). ** indicates $P < 0.01$ (Mann-Whitney). (**F**) Intracellular chymase expression in epithelial MCs (red), $CD38^{high}$ subepithelial MCs (orange), and $CD38^{low}$ subepithelial MCs (blue) versus isotype (gray). (**G**) Quantification of chymase expression in indicated MC subsets ($n = 5$ donors); *$P < 0.05$ and ***$P < 0.001$ (*t* test). (**H**) Intracellular fluorescein isothiocyanate (FITC)–avidin staining in epithelial MCs (red), $CD38^{high}$ subepithelial MCs (orange), and $CD38^{low}$ subepithelial MCs (blue). (**I**) Quantification of FITC-avidin fluorescence in indicated MC subsets ($n = 9$ donors); *$P < 0.05$ (*t* test).

respiratory intraepithelial MC transcriptional program. Treatment of primary cord blood MCs with IL-4, a T2 cytokine required for murine intraepithelial MC hyperplasia during helminth infection and food allergy (*42*, *43*), induces *IL17RB* expression along with other iMC_T transcripts. Although IL-4 did not up-regulate proliferation-associated transcripts in cord blood MCs, prior studies have shown that IL-4 markedly amplifies stem cell factor–dependent proliferation in human primary MCs from the intestine and peripheral blood (*53*, *54*). The finding that treatment with the IL-4Rα–blocking antibody dupilumab, highly efficacious for CRSwNP (*55*), sharply reduces *IL17RB* expression by the MC cluster further supports the concept that IL-4 contributes substantially to iMC_T hyperplasia and function. Epithelial signatures of IL-4/13 signaling correlated with MC concentration in our prior study of nasal polyposis (*22*), and this signature is also elevated in the lungs of asthmatics (*41*). Patients with fibrosis similarly exhibit enhanced T2 cytokine pathway activation (*40*). Ultimately, an analysis of whether therapeutic interventions for polyposis and asthma, including monoclonal antibody blockade of IL-4/13 (*56*, *57*), and CD117 inhibition (*2*) alter MC proliferation and transcriptional activity will allow definitive identification of tissue drivers of MC hyperplasia and differentiation.

MCs are thought to arise from rare agranular circulating $CD34^{+}Itg\beta7^{+}$ precursors (*13*). Although $Itg\beta7^{high}$ MCs were enriched in both aspirin-tolerant CRSwNP and AERD tissue compared with controls, these cells were $CD34^{-}$, contained cytoplasmic granules, and expressed tryptase, suggesting maturation. Although predominantly intraepithelial, $Itg\beta7^{high}$ MCs could be found within all populations and were transcriptionally indistinguishable from $Itg\beta7^{-}$ MCs within the same clusters. Thus, a portion of the MC population within nasal polyps, particularly iMC_T, may arise directly from recruited MC_P. Two additional clusters within the polyp MC pool were not expected based on prior histologic studies: one lacking signature transcripts and one undergoing proliferation. Both clusters expressed low levels of iMC_T and iMC_{TC} signature transcripts, suggesting that they were developmentally intermediate between the two polarized populations. CITE-seq analysis linked these "intermediate" MCs to the prominent expanded $CD117^{high}CD38^{high}$ MC pool, which by flow cytometry displayed variable chymase expression and avidin binding. $CD117^{hi}CD38^{hi}$ MCs accounted for 40 to 60% of CRSwNP tissue MCs were present (although reduced) in CRSsNP controls and were enriched for proliferation. Moreover, $Ki67^{+}$ MCs were substantially elevated in AERD and correlated with blood eosinophilia, a marker of T2 cytokine production (*58*). It is thus likely that MC hyperplasia results from a combination of $Itg\beta7^{high}$ MCp recruitment and in situ MC proliferation, with the contributions from the latter being magnified in more severe disease. The combination of polarization and proliferation suggests a similar paradigm to that observed with monocytes, which have innate effector capacity, mature, and take on distinct effector programs in response to local inflammatory signals, and are maintained within tissue through local IL-4–driven proliferation (*59*, *60*).

Although our transcriptomic analysis strongly suggests that the intermediate $CD117^{hi}CD38^{hi}$ MCs contributes to both iMC_T and iMC_{TC} hyperplasia, future studies will be required to determine whether these cells are capable of polarizing toward both observed MC effector phenotypes. Furthermore, although $CD117^{hi}CD38^{hi}$ MCs express similar levels of lipid mediator biosynthetic enzymes

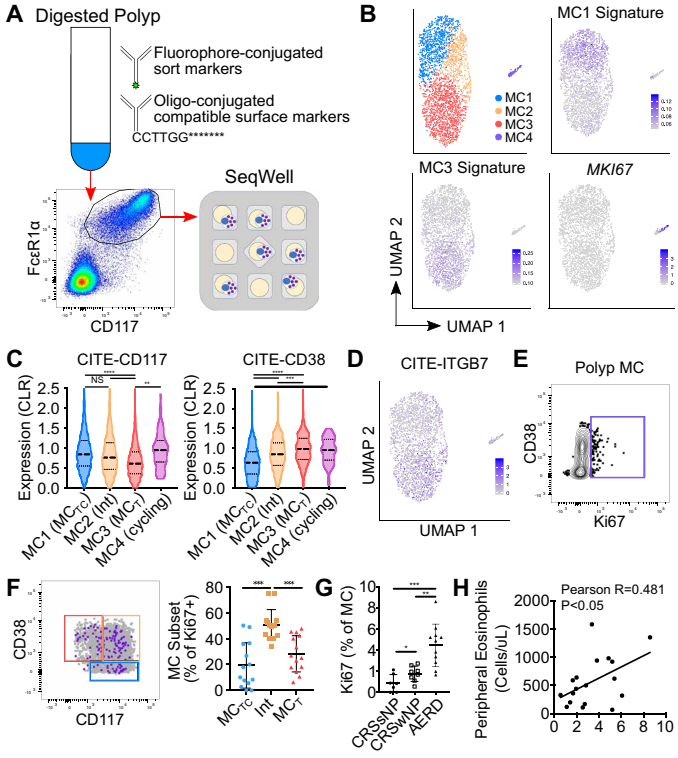

Fig. 7. Unpolarized MC proliferation underlies MC expansion in human nasal polyps. (**A**) Schematic approach for CITE-seq analysis of sorted polyp-derived MCs. (**B**) Identification of four clusters across 2902 MCs from two donors with expression of the MC1 and MC3 gene signatures (table S2) and *MKI67*. (**C**) Cell surface expression of CD117 and CD38 within each MC cluster [expressed as centered log ratio (CLR), line denotes median and quartiles]; $^{**}P < 1 \times 10^{-4}$, $^{***}P < 1 \times 10^{-12}$, and $^{****}P < 1 \times 10^{-15}$; NS, not significant (Mann-Whitney). (**D**) UMAP plot showing cell surface expression of Itgβ7 across nasal polyp MCs. (**E**) Representative plot of nuclear Ki67 in nasal polyp MCs. (**F**) Overlay showing $Ki67^+$ MCs (purple) and all MCs (gray) with flow gates defined in Fig. 6A (left). Quantification of $Ki67^+$ MCs by subset (right); $^{***}P < 0.001$ (*t* test). (**G**) Quantification of $Ki67^+$ MCs in indicated disease endotypes. $^{***}P < 0.00$ (*t* test). (**H**) Correlation of MC proliferation (Ki67 staining) and peripheral blood eosinophil counts across patients with polyp. Pearson $R = 0.481$, $P < 0.05$.

as iMC_T and iMC_{TC}, we were unable to directly assess their ability to generate inflammatory mediators. As a previous transcriptomic analysis of human circulating MC_P indicated that even agranular progenitors were enriched for *HGPDS* expression (*13*), it will be important to understand whether this means that MC lineage cells are capable of producing lipid mediators at all phases of development or whether, instead, the enzymes themselves are only translated after maturation. It is also unclear what role the three primary transcripts found to associate with the iMC_T across disease states, *CD38*, *GPR183*, and *IL17RB*, may play in MC biology. EBI2, encoded by *GPR183*, has been shown to participate in B cell and DC localization within tissues (*28*, *29*, *61*), suggesting a similar role in MCs. Although it is less clear what effects CD38 and IL-17RB may have on iMC_T biology, the identification of IL-4 as a signal capable of up-regulating both receptors in vitro provides critical insight for future studies exploring their roles.

In summary, through transcriptional and flow cytometric characterization of MC hyperplasia in T2 airway inflammation, we identify transcriptionally and phenotypically distinct MC subsets that potentially emerge from a novel, proliferative intermediate MC subtype. The polarized MC subtypes emerging from the intermediate subtype assume distinct transcriptional and morphologic characteristics based on their tissue microenvironment. The expansion of the intermediate subtype may be a critical determinant of disease severity, in turn reflecting perturbations in the surrounding stroma, mitogenic cytokines, and inflammatory mediators that likely exert a substantial additional influence on the MCs within each tissue microenvironment. Uncovering the drivers of this proliferative response and the tissue signals responsible for directing MC polarization will be critical for identifying therapeutic targets for T2 inflammation–associated diseases in which MC hyperplasia is prominent and MC effector responses play an important role.

MATERIALS AND METHODS

Study participants and design

Ethmoid sinus tissue was obtained from participants between the ages of 21 and 76 years, recruited from the Brigham and Women's Hospital (Boston, MA) Allergy and Immunology Clinic and Otolaryngology Clinic between May 2014 and September 2020 (table S1). This study was approved by the Institutional Review Board (IRB), with all study participants providing written consent. Tissue was collected at the time of elective endoscopic sinus surgery from patients with physician-diagnosed CRSwNP or CRSsNP. Patients with polyps included diagnoses of both aspirin-tolerant CRSwNP and aspirin-intolerant AERD. A diagnosis of AERD was suspected for patients with asthma, nasal polyposis, and a history of respiratory reaction after usage of cyclooxygenase inhibitors, and all diagnoses were confirmed via graded oral challenge with aspirin. Patients with cystic fibrosis and unilateral polyps were excluded. After no distinctions in MC characteristics between the two disease endotypes were noted beyond MC concentration and proliferation, the data were combined unless otherwise noted. Analysis was conducted in a nonblinded manner. Peripheral blood was obtained from patients without ethmoid sinus disease under the same protocol. Deidentified human skin samples were obtained from the Brigham and Women's Hospital Surgical Department under a separate IRB-approved protocol.

Flow cytometry, cell sorting, and analysis

Single-cell suspensions were resuspended in fluorescence-activated cell sorting (FACS) buffer [Hanks' balanced salt solution, Ca/Mg-free (Thermo Fisher Scientific) supplemented with 2% fetal calf serum, and 1 mM EDTA] before flow cytometric staining. MCs were sorted on a Sony SH800 cell sorter using Sony cell sorter software (Seq-Well) or a BD FACSAria Fusion cell sorter using BD FACSDiva software (histologic assessment). For all flow cytometry not involving cell sorting, cells were analyzed on a BD LSR II Fortessa or BD FACSCanto II using BD FACSDiva software.

Cytologic analysis

To minimize cell loss, sorted MCs were placed on a glass slide at a concentration of 1000 cells in 10 μl. Slides were quickly dried using a plate warmer at the lowest setting. For granule visualization, cells were stained with 100 μl of toluidine blue solution (94.2% H_2O, 5.8% concentrated HCl, and 0.5 g of toluidine blue) for 30 s and washed using deionized H_2O. For protease immunostaining, cells were fixed with Carnoy's fixative as previously described (*62*).

Histologic analysis

Nasal polyp biopsies were fixed in 4% paraformaldehyde and embedded in paraffin, and 6-μm sections were cut for histologic analysis. Tissue sections were deparaffinized and rehydrated. Slides were quenched with sodium borohydride (1 mg/ml) three times on ice for 10 min each. Antigen retrieval was performed with Target Retrieval Solution (pH 9) (Agilent Technologies Inc.) at 97°C for 35 min. Microscopy and photography were done using Olympus BX-41 system microscope and Olympus DP-71 camera.

scRNA-seq and analysis

After obtaining single-cell suspensions from freshly resected sinus tissue, we used the Seq-Well platform for massively parallel scRNA-seq to capture transcriptomes of sorted MCs on barcoded mRNA capture beads (*27*), described in greater detail in Supplementary Methods. Read alignment was performed as in Macosko *et al.* (*63*). Unique molecular identifier (UMI)–collapsed data were used as input into Seurat (*64*) (https://github.com/satijalab/seurat) for analysis. Before incorporating a sample into our merged dataset, we individually inspected the cell-by-gene matrix of each as a Seurat object. For analysis of all sequenced samples, we merged UMI matrices across all genes detected to generate a matrix containing all cells detected (n = 8228 cells and 25,104 genes). This table was then used to set up the Seurat object in which any cell with at least 200 unique genes was retained and any gene expressed in at least three cells was retained. Cells with greater than 10% mitochondrial genes or UMI counts less than 200 and greater than 2500 were removed from analysis. The total number of cells passing these filters captured across all patients was 7355 cells with 18,102 genes, averaging 2699 cells per sample with a range between 221 and 2359 cells. Before performing dimensionality reduction, data were log normalized with a scale factor of 10,000, scaled, and centered, and a list of 2000 most variable genes was generated by using the "vst" selection setting. We then performed principal components analysis using variable genes. A shared nearest neighbor (SNN) graph and uniform manifold approximation and projection embedding (UMAP) were constructed using the first nine principal components based on the inflection point of the elbow plot. We used FindClusters (which uses an SNN modularity optimization–based clustering algorithm) with a resolution of 0.4 and RunUMAP using default settings to identify 10 clusters across the six input samples. Additional analysis information can be found in Supplementary Methods.

CITE-seq computational pipelines and analysis

CITE-seq methodology can be found in Supplementary Methods. For analysis, CITE-seq tag counting and demultiplexed antibody-derived tag (ADT) reads were processed using the CITE-seq-Count package version 1.4.2. Reads were matched with their corresponding ADT sequences and assigned to cell barcodes within a whitelist of cells that contained between 200 and 2500 mRNA UMIs. Once binned by cell barcode, ADT reads were collapsed by their 8–base pair UMI.

For data analysis, one Seurat object was created per sample. Cells with UMI counts less than 200 and greater than 2500 were removed from the analysis. For both experiments, data were log-normalized with a scale factor of 10,000, scaled, and centered, and the 2000 most variable transcripts were determined using the FindVariableFeatures function. Tag counts for ADTs were scaled and centered before center log ratio normalization. Contaminating cell populations were computationally removed from each object as described in the Cell Type Identification, and the two experiments were integrated within Seurat using the Harmony software package (*65*). For constructing a SNN graph and UMAP embedding, we used the first 10 principal components, reflecting the inflection point of the elbow plot. We used FindClusters with a resolution of 0.4 and RunUMAP using default settings to identify four clusters across the two input samples.

Statistical analysis

A number of samples included in analyses are listed throughout figure legends and represent distinct biological samples. Source data are provided in table S7. No samples or cells meeting quality thresholds were excluded from analyses. Statistical analyses were performed using GraphPad Prism v7.0c and Seurat 3.0.1 implemented in RStudio. Some violin plots were generated using Graphpad Prism using data exported from Seurat to allow display of median and quartile values. Paired t tests were used when comparing protein expression across multiple subsets within individual patients and are indicated by linked points. Unpaired two-tailed t tests were for comparisons of data found to be normally distributed using the D'Agostino and Pearson test. For all other data, the Mann-Whitney U tests were used for comparisons.

SUPPLEMENTARY MATERIALS

immunology.sciencemag.org/cgi/content/full/6/56/eabb7221/DC1
Supplementary Methods
Fig. S1. In-depth characterization of nasal polyp MCs.
Fig. S2. Characterization of nasal polyp MC protease phenotype and localization.
Fig. S3. Characterization of sorted cells through scRNA-seq.
Fig. S4. Immunohistologic localization of EBI2-expressing MCs.
Fig. S5. Identification of MCs in three IPF scRNA-seq datasets.
Fig. S6. Identification of an asthma-enriched CD38^{high} MC cluster.
Fig. S7. Influence of dupilumab on nasal polyp MC transcript expression.
Fig. S8. Schematic representation of strategy for evaluating the transcriptome of Itgβ7^{high} MCs.
Fig. S9. Proposed model for MC homeostasis and hyperplasia in human sinus mucosa.
Table S1. Patient information.
Table S2. Gene lists derived from literature and databases used for scoring.
Table S3. Cell-by-gene matrix (raw) for sorted MCs from six polyp donors.
Table S4. Cluster defining marker genes, MC subset defining genes, and differential expression full gene lists presented in manuscript.
Table S5. Cluster defining marker genes for scRNA-seq datasets from the human IPF lung atlas and asthma versus healthy donors.
Table S6. Differential gene expression analysis for human umbilical cord–derived MCs treated with IL-4 or vehicle for 96 hours.
Table S7. Source data for figures.

View/request a protocol for this paper from *Bio-protocol*.

REFERENCES AND NOTES

1. K. Mukai, M. Tsai, H. Saito, S. J. Galli, Mast cells as sources of cytokines, chemokines, and growth factors. *Immunol. Rev.* **282**, 121–150 (2018).
2. K. N. Cahill, H. R. Katz, J. Cui, J. Lai, S. Kazani, A. Crosby-Thompson, D. Garofalo, M. Castro, N. Jarjour, E. DiMango, S. Erzurum, J. L. Trevor, K. Shenoy, V. M. Chinchilli, M. E. Wechsler, T. M. Laidlaw, J. A. Boyce, E. Israel, KIT inhibition by imatinib in patients with severe refractory asthma. *N. Engl. J. Med.* **376**, 1911–1920 (2017).
3. D. Voehringer, Protective and pathological roles of mast cells and basophils. *Nat. Rev. Immunol.* **13**, 362–375 (2013).
4. C. K. Andersson, M. Mori, L. Bjermer, C.-G. Löfdahl, J. S. Erjefält, Novel site-specific mast cell subpopulations in the human lung. *Thorax* **64**, 297–305 (2009).
5. A. A. Irani, N. M. Schechter, S. S. Craig, G. DeBlois, L. B. Schwartz, Two types of human mast cells that have distinct neutral protease compositions. *Proc. Natl. Acad. Sci. U.S.A.* **83**, 4464–4468 (1986).
6. R. Gentek, C. Ghigo, G. Hoeffel, M. J. Bulle, R. Msallam, G. Gautier, P. Launay, J. Chen, F. Ginhoux, M. Bajénoff, Hemogenic endothelial fate mapping reveals dual developmental origin of mast cells. *Immunity* **48**, 1160–1171.e5 (2018).

7. Z. Li, S. Liu, J. Xu, X. Zhang, D. Han, J. Liu, M. Xia, L. Yi, Q. Shen, S. Xu, L. Lu, X. Cao, Adult connective tissue-resident mast cells originate from late erythro-myeloid progenitors. *Immunity* **49**, 640–653.e5 (2018).
8. M. F. Gurish, H. Tao, J. P. Abonia, A. Arya, D. S. Friend, C. M. Parker, K. F. Austen, Intestinal mast cell progenitors require CD49dβ7 (α4β7 integrin) for tissue-specific homing. *J. Exp. Med.* **194**, 1243–1252 (2001).
9. J. P. Abonia, J. Hallgren, T. Jones, T. Shi, Y. Xu, P. Koni, R. A. Flavell, J. A. Boyce, K. F. Austen, M. F. Gurish, Alpha-4 integrins and VCAM-1, but not MAdCAM-1, are essential for recruitment of mast cell progenitors to the inflamed lung. *Blood* **108**, 1588–1594 (2006).
10. L. G. Bankova, D. F. Dwyer, A. Y. Liu, K. F. Austen, M. F. Gurish, Maturation of mast cell progenitors to mucosal mast cells during allergic pulmonary inflammation in mice. *Mucosal Immunol.* **8**, 596–606 (2015).
11. D. F. Dwyer, N. A. Barrett, K. F. Austen; Immunological Genome Project Consortium, Expression profiling of constitutive mast cells reveals a unique identity within the immune system. *Nat. Immunol.* **17**, 878–887 (2016).
12. W. Xing, K. F. Austen, M. F. Gurish, T. G. Jones, Protease phenotype of constitutive connective tissue and of induced mucosal mast cells in mice is regulated by the tissue. *Proc. Natl. Acad. Sci. U.S.A.* **108**, 14210–14215 (2011).
13. J. S. Dahlin, A. Malinovschi, H. Öhrvik, M. Sandelin, C. Janson, K. Alving, J. Hallgren, Lin^- $CD34^{hi}$ $CD117^{int/hi}$ $Fc\varepsilon RI^+$ cells in human blood constitute a rare population of mast cell progenitors. *Blood* **127**, 383–391 (2016).
14. S. Zheng, E. Papalexi, A. Butler, W. Stephenson, R. Satija, Molecular transitions in early progenitors during human cord blood hematopoiesis. *Mol. Syst. Biol.* **14**, e8041 (2018).
15. R. H. Dougherty, S. S. Sidhu, K. Raman, M. Solon, O. D. Solberg, G. H. Caughey, P. G. Woodruff, J. V. Fahy, Accumulation of intraepithelial mast cells with a unique protease phenotype in T_H2-high asthma. *J. Allergy Clin. Immunol.* **125**, 1046–1053.e8 (2010).
16. S. Balzar, M. L. Fajt, S. A. A. Comhair, S. C. Erzurum, E. Bleecker, W. W. Busse, M. Castro, B. Gaston, E. Israel, L. B. Schwartz, D. Curran-Everett, C. G. Moore, S. E. Wenzel, Mast cell phenotype, location, and activation in severe asthma. Data from the Severe Asthma Research Program. *Am. J. Respir. Crit. Care Med.* **183**, 299–309 (2011).
17. T. Takabayashi, A. Kato, A. T. Peters, L. A. Suh, R. Carter, J. Norton, L. C. Grammer, B. K. Tan, R. K. Chandra, D. B. Conley, R. C. Kern, S. Fujieda, R. P. Schleimer, Glandular mast cells with distinct phenotype are highly elevated in chronic rhinosinusitis with nasal polyps. *J. Allergy Clin. Immunol.* **130**, 410–420.e5 (2012).
18. J. P. Abonia, C. Blanchard, B. B. Butz, H. F. Rainey, M. H. Collins, K. Stringer, P. E. Putnam, M. E. Rothenberg, Involvement of mast cells in eosinophilic esophagitis. *J. Allergy Clin. Immunol.* **126**, 140–149 (2010).
19. C. E. Brightling, P. Bradding, F. A. Symon, S. T. Holgate, A. J. Wardlaw, I. D. Pavord, Mast-cell infiltration of airway smooth muscle in asthma. *N. Engl. J. Med.* **346**, 1699–1705 (2002).
20. S. Siddiqui, V. Mistry, C. Doe, K. Roach, A. Morgan, A. Wardlaw, I. Pavord, P. Bradding, C. Brightling, Airway hyperresponsiveness is dissociated from airway wall structural remodeling. *J. Allergy Clin. Immunol.* **122**, 335–341 (2008).
21. S. Finotto, J. Dolovich, J. A. Denburg, M. Jordana, J. S. Marshall, Functional heterogeneity of mast cells isolated from different microenvironments within nasal polyp tissue. *Clin. Exp. Immunol.* **95**, 343–350 (1994).
22. J. Ordovas-Montanes, D. F. Dwyer, S. K. Nyquist, K. M. Buchheit, M. Vukovic, C. Deb, M. H. Wadsworth II, T. K. Hughes, S. W. Kazer, E. Yoshimoto, K. N. Cahill, N. Bhattacharyya, H. R. Katz, B. Berger, T. M. Laidlaw, J. A. Boyce, N. A. Barrett, A. K. Shalek, Allergic inflammatory memory in human respiratory epithelial progenitor cells. *Nature* **560**, 649–654 (2018).
23. A. A. White, D. D. Stevenson, Aspirin-exacerbated respiratory disease. *N. Engl. J. Med.* **379**, 1060–1070 (2018).
24. K. M. Buchheit, K. N. Cahill, H. R. Katz, K. C. Murphy, C. Feng, K. Lee-Sarwar, J. Lai, N. Bhattacharyya, E. Israel, J. A. Boyce, T. M. Laidlaw, Thymic stromal lymphopoietin controls prostaglandin D2 generation in patients with aspirin-exacerbated respiratory disease. *J. Allergy Clin. Immunol.* **137**, 1566–1576.e5 (2016).
25. K. L. Cepek, S. K. Shaw, C. M. Parker, G. J. Russell, J. S. Morrow, D. L. Rimm, M. B. Brenner, Adhesion between epithelial cells and T lymphocytes mediated by E-cadherin and the $\alpha^E\beta_7$ integrin. *Nature* **372**, 190–193 (1994).
26. C. Berlin, E. L. Berg, M. J. Briskin, D. P. Andrew, P. J. Kilshaw, B. Holzmann, I. L. Weissman, A. Hamann, E. C. Butcher, α4β7 integrin mediates lymphocyte binding to the mucosal vascular addressin MAdCAM-1. *Cell* **74**, 185–195 (1993).
27. T. M. Gierahn, M. H. Wadsworth II, T. K. Hughes, B. D. Bryson, A. Butler, R. Satija, S. Fortune, J. C. Love, A. K. Shalek, Seq-Well: Portable, low-cost RNA sequencing of single cells at high throughput. *Nat. Methods* **14**, 395–398 (2017).
28. S. Hannedouche, J. Zhang, T. Yi, W. Shen, D. Nguyen, J. P. Pereira, D. Guerini, B. U. Baumgarten, S. Roggo, B. Wen, R. Knochenmuss, S. Noël, F. Gessier, L. M. Kelly, M. Vanek, S. Laurent, I. Preuss, C. Miault, I. Christen, R. Karuna, W. Li, D.-I. Koo, T. Suply, C. Schmedt, E. C. Peters, R. Falchetto, A. Katopodis, C. Spanka, M.-O. Roy, M. Detheux, Y. A. Chen, P. G. Schultz, C. Y. Cho, K. Seuwen, J. G. Cyster, A. W. Sailer, Oxysterols direct immune cell migration via EBI2. *Nature* **475**, 524–527 (2011).
29. C. Liu, X. V. Yang, J. Wu, C. Kuei, N. S. Mani, L. Zhang, J. Yu, S. W. Sutton, N. Qin, H. Banie, L. Karlsson, S. Sun, T. W. Lovenberg, Oxysterols direct B-cell migration through EBI2. *Nature* **475**, 519–523 (2011).
30. A. Collison, J. Li, A. P. de Siqueira, J. Zhang, H. D. Toop, J. C. Morris, P. S. Foster, J. Mattes, Tumor necrosis factor-related apoptosis-inducing ligand regulates hallmark features of airways remodeling in allergic airways disease. *Am. J. Respir. Cell Mol. Biol.* **51**, 86–93 (2014).
31. M. Weckmann, A. Collison, J. L. Simpson, M. V. Kopp, P. A. B. Wark, M. J. Smyth, H. Yagita, K. I. Matthaei, N. Hansbro, B. Whitehead, P. G. Gibson, P. S. Foster, J. Mattes, Critical link between TRAIL and CCL20 for the activation of T_H2 cells and the expression of allergic airway disease. *Nat. Med.* **13**, 1308–1315 (2007).
32. I. Shalev, H. Liu, C. Koscik, A. Bartczak, M. Javadi, K. M. Wong, A. Maknojia, W. He, M. F. Liu, J. Diao, E. Winter, J. Manuel, D. McCarthy, M. Cattral, J. Gommerman, D. A. Clark, M. J. Phillips, R. R. Gorczynski, L. Zhang, G. Downey, D. Grant, M. I. Cybulsky, G. Levy, Targeted deletion of fgl2 leads to impaired regulatory T cell activity and development of autoimmune glomerulonephritis. *J. Immunol.* **180**, 249–260 (2008).
33. N. Martin, A. Ruddick, G. K. Arthur, H. Wan, L. Woodman, C. E. Brightling, D. J. L. Jones, I. D. Pavord, P. Bradding, Primary human airway epithelial cell-dependent inhibition of human lung mast cell degranulation. *PLOS ONE* **7**, e43545 (2012).
34. F. H. Hsieh, P. Sharma, A. Gibbons, T. Goggans, S. C. Erzurum, S. J. Haque, Human airway epithelial cell determinants of survival and functional phenotype for primary human mast cells. *Proc. Natl. Acad. Sci. U.S.A.* **102**, 14380–14385 (2005).
35. K. D. Chhiba, C.-L. Hsu, S. Berdnikovs, P. J. Bryce, Transcriptional heterogeneity of mast cells and basophils upon activation. *J. Immunol.* **198**, 4868–4878 (2017).
36. N. Neumark (2019); www.ipfcellatlas.com.
37. A. C. Habermann, A. J. Gutierrez, L. T. Bui, S. L. Yahn, N. I. Winters, C. L. Calvi, L. Peter, M.-I. Chung, C. J. Taylor, C. Jetter, L. Raju, J. Roberson, G. Ding, L. Wood, J. M. S. Sucre, B. W. Richmond, A. P. Serezani, W. J. McDonnell, S. B. Mallal, M. J. Bacchetta, J. E. Loyd, C. M. Shaver, L. B. Ware, R. Bremner, R. Walia, T. S. Blackwell, N. E. Banovich, J. A. Kropski, Single-cell RNA sequencing reveals profibrotic roles of distinct epithelial and mesenchymal lineages in pulmonary fibrosis. *Sci. Adv.* **6**, eaba1972 (2020).
38. T. S. Adams, J. C. Schupp, S. Poli, E. A. Ayaub, N. Neumark, F. Ahangari, S. G. Chu, B. A. Raby, G. De Iuliis, M. Januszyk, Q. Duan, H. A. Arnett, A. Siddiqui, G. R. Washko, R. Homer, X. Yan, I. O. Rosas, N. Kaminski, Single-cell RNA-seq reveals ectopic and aberrant lung-resident cell populations in idiopathic pulmonary fibrosis. *Sci. Adv.* **6**, eaba1983 (2020).
39. C. Morse, T. Tabib, J. Sembrat, K. L. Buschur, H. T. Bittar, E. Valenzi, Y. Jiang, D. J. Kass, K. Gibson, W. Chen, A. Mora, P. V. Benos, M. Rojas, R. Lafyatis, Proliferating SPP1/MERTK-expressing macrophages in idiopathic pulmonary fibrosis. *Eur. Respir. J.* **54**, 1802441 (2019).
40. L. A. Murray, H. Zhang, S. R. Oak, A. L. Coelho, A. Herath, K. R. Flaherty, J. Lee, M. Bell, D. A. Knight, F. J. Martinez, M. A. Sleeman, E. L. Herzog, C. M. Hogaboam, Targeting interleukin-13 with tralokinumab attenuates lung fibrosis and epithelial damage in a humanized SCID idiopathic pulmonary fibrosis model. *Am. J. Respir. Cell Mol. Biol.* **50**, 985–994 (2014).
41. F. A. Vieira Braga, G. Kar, M. Berg, O. A. Carpaij, K. Polanski, L. M. Simon, S. Brouwer, T. Gomes, L. Hesse, J. Jiang, E. S. Fasouli, M. Efremova, R. Vento-Tormo, C. Talavera-López, M. R. Jonker, K. Affleck, S. Palit, P. M. Strzelecka, H. V. Firth, K. T. Mahbubani, A. Cvejic, K. B. Meyer, K. Saeb-Parsy, M. Luinge, C.-A. Brandsma, W. Timens, I. Angelidis, M. Strunz, G. H. Koppelman, A. J. van Oosterhout, H. B. Schiller, F. J. Theis, M. van den Berge, M. C. Nawijn, S. A. Teichmann, A cellular census of human lungs identifies novel cell states in health and in asthma. *Nat. Med.* **25**, 1153–1163 (2019).
42. O. T. Burton, A. R. Darling, J. S. Zhou, M. Noval-Rivas, T. G. Jones, M. F. Gurish, T. A. Chatila, H. C. Oettgen, Direct effects of IL-4 on mast cells drive their intestinal expansion and increase susceptibility to anaphylaxis in a murine model of food allergy. *Mucosal Immunol.* **6**, 740–750 (2013).
43. K. B. Madden, L. Whitman, C. Sullivan, W. C. Gause, J. F. Urban Jr., I. M. Katona, F. D. Finkelman, T. Shea-Donohue, Role of STAT6 and mast cells in IL-4- and IL-13-induced alterations in murine intestinal epithelial cell function. *J. Immunol.* **169**, 4417–4422 (2002).
44. T. K. Hughes, M. H. Wadsworth, T. M. Gierahn, T. Do, D. Weiss, P. R. Andrade, F. Ma, B. J. de Andrade Silva, S. Shao, L. C. Tsoi, J. Ordovas-Montanes, J. E. Gudjonsson, R. L. Modlin, J. C. Love, A. K. Shalek, Second-strand synthesis-based massively parallel scRNA-Seq reveals cellular states and molecular features of human inflammatory skin pathologies. *Immunity* **53**, 878–894.e7 (2020).
45. C. A. Oskeritzian, W. Zhao, H.-K. Min, H.-Z. Xia, A. Pozez, J. Kiev, L. B. Schwartz, Surface CD88 functionally distinguishes the MCTC from the MCT type of human lung mast cell. *J. Allergy Clin. Immunol.* **115**, 1162–1168 (2005).
46. D. Fujisawa, J.-I. Kashiwakura, H. Kita, Y. Kikukawa, Y. Fujitani, T. Sasaki-Sakamoto, K. Kuroda, S. Nunomura, K. Hayama, T. Terui, C. Ra, Y. Okayama, Expression of Mas-related gene X2 on mast cells is upregulated in the skin of patients with severe chronic urticaria. *J. Allergy Clin. Immunol.* **134**, 622–633.e9 (2014).

47. K. J. Travaglini, A. N. Nabhan, L. Penland, R. Sinha, A. Gillich, R. V. Sit, S. Chang, S. D. Conley, Y. Mori, J. Seita, G. J. Berry, J. B. Shrager, R. J. Metzger, C. S. Kuo, N. Neff, I. L. Weissman, S. R. Quake, M. A. Krasnow, A molecular cell atlas of the human lung from single-cell RNA sequencing. *Nature* **587**, 619–625 (2020).
48. W. C. Kett, R. I. W. Osmond, L. Moe, S. E. Skett, B. F. Kinnear, D. R. Coombe, Avidin is a heparin-binding protein. Affinity, specificity and structural analysis. *Biochim. Biophys. Acta* **1620**, 225–234 (2003).
49. N. Weidner, K. F. Austen, Heterogeneity of mast cells at multiple body sites. Fluorescent determination of avidin binding and immunofluorescent determination of chymase, tryptase, and carboxypeptidase content. *Pathol. Res. Pract.* **189**, 156–162 (1993).
50. M. Stoeckius, C. Hafemeister, W. Stephenson, B. Houck-Loomis, P. K. Chattopadhyay, H. Swerdlow, R. Satija, P. Smibert, Simultaneous epitope and transcriptome measurement in single cells. *Nat. Methods* **14**, 865–868 (2017).
51. E. Motakis, S. Guhl, Y. Ishizu, M. Itoh, H. Kawaji, M. de Hoon, T. Lassmann, P. Carninci, Y. Hayashizaki, T. Zuberbier, A. R. R. Forrest, M. Babina; FANTOM Consortium, Redefinition of the human mast cell transcriptome by deep-CAGE sequencing. *Blood* **123**, e58–e67 (2014).
52. W. Füreder, H. Agis, M. Willheim, H. C. Bankl, U. Maier, K. Kishi, M. R. Müller, K. Czerwenka, T. Radaszkiewicz, J. H. Butterfield, G. W. Klappacher, W. R. Sperr, M. Oppermann, K. Lechner, P. Valent, Differential expression of complement receptors on human basophils and mast cells. Evidence for mast cell heterogeneity and CD88/C5aR expression on skin mast cells. *J. Immunol.* **155**, 3152–3160 (1995).
53. S. C. Bischoff, G. Sellge, A. Lorentz, W. Sebald, R. Raab, M. P. Manns, IL-4 enhances proliferation and mediator release in mature human mast cells. *Proc. Natl. Acad. Sci. U.S.A.* **96**, 8080–8085 (1999).
54. M. Kulka, D. D. Metcalfe, High-resolution tracking of cell division demonstrates differential effects of T_H1 and T_H2 cytokines on SCF-dependent human mast cell production in vitro: Correlation with apoptosis and Kit expression. *Blood* **105**, 592–599 (2005).
55. C. Bachert, J. K. Han, M. Desrosiers, P. W. Hellings, N. Amin, S. E. Lee, J. Mullol, L. S. Greos, J. V. Bosso, T. M. Laidlaw, A. U. Cervin, J. F. Maspero, C. Hopkins, H. Olze, G. W. Canonica, P. Paggiaro, S. H. Cho, W. J. Fokkens, S. Fujieda, M. Zhang, X. Lu, C. Fan, S. Draikiwicz, S. A. Kamat, A. Khan, G. Pirozzi, N. Patel, N. M. H. Graham, M. Ruddy, H. Staudinger, D. Weinreich, N. Stahl, G. D. Yancopoulos, L. P. Mannent, Efficacy and safety of dupilumab in patients with severe chronic rhinosinusitis with nasal polyps (LIBERTY NP SINUS-24 and LIBERTY NP SINUS-52): Results from two multicentre, randomised, double-blind, placebo-controlled, parallel-group phase 3 trials. *Lancet* **394**, 1638–1650 (2019).
56. S. Wenzel, M. Castro, J. Corren, J. Maspero, L. Wang, B. Zhang, G. Pirozzi, E. R. Sutherland, R. R. Evans, V. N. Joish, L. Eckert, N. M. H. Graham, N. Stahl, G. D. Yancopoulos, M. Louis-Tisserand, A. Teper, Dupilumab efficacy and safety in adults with uncontrolled persistent asthma despite use of medium-to-high-dose inhaled corticosteroids plus a long-acting β2 agonist: A randomised double-blind placebo-controlled pivotal phase 2b dose-ranging trial. *Lancet* **388**, 31–44 (2016).
57. H. G. Ortega, M. C. Liu, I. D. Pavord, G. G. Brusselle, J. M. FitzGerald, A. Chetta, M. Humbert, L. E. Katz, O. N. Keene, S. W. Yancey, P. Chanez; MENSA Investigators, Mepolizumab treatment in patients with severe eosinophilic asthma. *N. Engl. J. Med.* **371**, 1198–1207 (2014).
58. C. Walker, R. K. Braun, C. Boer, C. Kroegel, J. C. Virchow, T. T. Hansel, Cytokine control of eosinophils in pulmonary diseases. *J. Allergy Clin. Immunol.* **94**, 1262–1271 (1994).
59. S. J. Jenkins, D. Ruckerl, P. C. Cook, L. H. Jones, F. D. Finkelman, N. van Rooijen, A. S. MacDonald, J. E. Allen, Local macrophage proliferation, rather than recruitment from the blood, is a signature of T_H2 inflammation. *Science* **332**, 1284–1288 (2011).
60. S. Gordon, F. O. Martinez, Alternative activation of macrophages: Mechanism and functions. *Immunity* **32**, 593–604 (2010).
61. T. Yi, J. G. Cyster, EBI2-mediated bridging channel positioning supports splenic dendritic cell homeostasis and particulate antigen capture. *eLife* **2**, e00757 (2013).
62. T. M. Laidlaw, J. W. Steinke, A. M. Tiñana, C. Feng, W. Xing, B. K. Lam, S. Paruchuri, J. A. Boyce, L. Borish, Characterization of a novel human mast cell line that responds to stem cell factor and expresses functional FcεRI. *J. Allergy Clin. Immunol.* **127**, 815–822. e1-5 (2011).
63. E. Z. Macosko, A. Basu, R. Satija, J. Nemesh, K. Shekhar, M. Goldman, I. Tirosh, A. R. Bialas, N. Kamitaki, E. M. Martersteck, J. J. Trombetta, D. A. Weitz, J. R. Sanes, A. K. Shalek, A. Regev, S. A. McCarroll, Highly parallel genome-wide expression profiling of individual cells using nanoliter droplets. *Cell* **161**, 1202–1214 (2015).
64. R. Satija, J. A. Farrell, D. Gennert, A. F. Schier, A. Regev, Spatial reconstruction of single-cell gene expression data. *Nat. Biotechnol.* **33**, 495–502 (2015).
65. I. Korsunsky, N. Millard, J. Fan, K. Slowikowski, F. Zhang, K. Wei, Y. Baglaenko, M. Brenner, P.-r. Loh, S. Raychaudhuri, Fast, sensitive and accurate integration of single-cell data with Harmony. *Nat. Methods* **16**, 1289–1296 (2019).

Acknowledgments: We thank E. Lewis and N. Hallen for technical support in preparing tissue digests, the Broad Genomics Platform and Robert Chase of the BWH Channing Division of Network Medicine for RNA-seq assistance with CBMCs, members of the Shalek Laboratory for experimental and computational advice, and M. Morrison and F. Al Haddad for administrative support. **Funding:** J.A.B. was supported by NIH grants R37AI052353, R01AI136041, R01AI130109, R01HL136209, and U19 AI095219; N.A.B. by NIH grants R01HL120952, R01AI134989, U19AI095219, and Steven and Judy Kaye Young Innovators Award; A.K.S. by the Searle Scholars Program, the Beckman Young Investigator Program, the Pew-Stewart Scholars Program for Cancer Research, a Sloan Fellowship in Chemistry, the NIH (5U24AI118672), and the Bill and Melinda Gates Foundation; T.M.L. by NIH grants R01HL128241 and U19AI095219; M.C.N. acknowledges funding from the Netherlands Lung Foundation project nos. 5.1.14.020 and 4.1.18.226 and the European Union's H2020 Research and Innovation Program under grant agreement no. 874656 (discovAIR) and grant number CZF2019-002438 from the Chan Zuckerberg Initiative Foundation awarded to the HCA Lung Seed Network. K.M.B. was supported by NIH AADCRC Opportunity Fund Award U19AI070535; J.O.-M. is a New York Stem Cell Foundation–Robertson Investigator. J.O.-M. was supported by the Richard and Susan Smith Family Foundation, the HHMI Damon Runyon Cancer Research Foundation Fellowship (DRG-2274-16), the AGA Research Foundation's AGA-Takeda Pharmaceuticals Research Scholar Award in IBD-AGA2020-13-01, the HDDC Pilot and Feasibility P30 DK034854, the Food Allergy Science Initiative, and The New York Stem Cell Foundation; D.F.D. was supported by T32 AI007306 (to J.A.B.), NIH AADCRC Opportunity Fund Award U19AI070535 and K22 AI146281, and by contributions from the Vinik family. **Author contributions:** J.O.-M., D.F.D., S.J.A., T.M.L., A.K.S., N.A.B., and J.A.B. designed the study. N.B. and R.E.R. performed surgeries. J.O.-M., D.F.D., S.J.A., M.V., T.K.H., K.M.B., and M.P.G., collected patient samples and performed single-cell experiments. D.F.D., T.D., and M.P.G. conducted validation studies. C.F. conducted in vitro CBMC stimulus experiments. H.R.K. and J.L. performed histologic analyses. M.C.N., M.B., and M.v.d.B. conducted scRNA-seq analysis of asthma-derived MCs. D.F.D., J.O.-M., S.J.A., and S.K.N. analyzed data. J.O.-M., D.F.D., S.J.A., A.K.S., N.A.B., and J.A.B. interpreted data. J.O.-M., D.F.D., S.J.A., A.K.S., N.A.B., and J.A.B. wrote the manuscript, with input from all authors. **Competing interests:** J.O.-M. reports compensation for consulting services with Cellarity and Hovione. R.E.R. reports compensation for consulting services with Roche Genentech and Gossamer pharmaceuticals. N.A.B. reports compensation for consulting services for Regeneron. A.K.S. reports compensation for consulting and/or SAB membership from Merck, Honeycomb Biotechnologies, Cellarity, Repertoire Immune Medicines, Ochre Bio, Hovione, and Dahlia Biosciences. The other authors declare that they have no competing interests. **Data and materials availability:** A cell-by-gene matrix generated from sorted nasal polyp–derived MC and analyzed during the current study is available along with the manuscript as table S3. scRNA-seq raw data in FASTQ format have been deposited in dbGaP under accession no. phs002333.v1.p1. Bulk sequencing data have been deposited in the Gene Expression Omnibus under accession no. GSE165804.

Submitted 13 March 2020
Accepted 28 January 2021
Published 26 February 2021
10.1126/sciimmunol.abb7221

Citation: D. F. Dwyer, J. Ordovas-Montanes, S. J. Allon, K. M. Buchheit, M. Vukovic, T. Derakhshan, C. Feng, J. Lai, T. K. Hughes, S. K. Nyquist, M. P. Giannetti, B. Berger, N. Bhattacharyya, R. E. Roditi, H. R. Katz, M. C. Nawijn, M. Berg, M. van den Berge, T. M. Laidlaw, A. K. Shalek, N. A. Barrett, J. A. Boyce, Human airway mast cells proliferate and acquire distinct inflammation-driven phenotypes during type 2 inflammation. *Sci. Immunol.* **6**, eabb7221 (2021).

Science Immunology

Human airway mast cells proliferate and acquire distinct inflammation-driven phenotypes during type 2 inflammation

Daniel F. DwyerJose Ordovas-MontanesSamuel J. AllonKathleen M. BuchheitMarko VukovicTahereh DerakhshanChunli FengJuying LaiTravis K. HughesSarah K. NyquistMatthew P. GiannettiBonnie BergerNeil BhattacharyyaRachel E. RoditiHoward R. KatzMartijn C. NawijnMarijn BergMaarten van den BergeTanya M. LaidlawAlex K. ShalekNora A. BarrettJoshua A. Boyce

Sci. Immunol., 6 (56), eabb7221. • DOI: 10.1126/sciimmunol.abb7221

Mast cell spectrum

Mast cells (MCs), key players in type 2 (T2) allergic airway diseases such as chronic rhinosinusitis with nasal polyposis (CRSwNP), have mainly been characterized into different subsets based on protease content. Dwyer *et al.* have used flow cytometry and single-cell RNA-sequencing (scRNA-seq) to carry out a detailed study of human MC hyperplasia in CRSwNP. Relative to control tissue from patients with CRS lacking polyps, mature epithelial MCs that express tryptase (MCT), subepithelial MCs that express tryptase and chymase (MCTC), and CD38$^+$CD117$^+$ MCs with an intermediate phenotype between MCT and MCTC all expanded in polyps of patients with CRSwNP. These results suggest that local proliferation of CD38$^+$CD117$^+$ MCs is linked to both mature MC subsets and contributes to T2 disease.

Science Immunology (ISSN 2470-9468) is published by the American Association for the Advancement of Science. 1200 New York Avenue NW, Washington, DC 20005. The title *Science Immunology* is a registered trademark of AAAS.